Separating Radiation and Thermal Effects on Lateral PNP Bipolar Junction Transistors Operating in the Space Environment

By

Michael J. Campola

A Thesis Presented in Partial Fulfillment
of the Requirements for the Degree
Master of Science

Approved November 2011 by the
Graduate Supervisory Committee:

Hugh J. Barnaby, Chair
Dragica Vasileska
K. E. Holbert

ARIZONA STATE UNIVERSITY

December 2011

ABSTRACT

Radiation-induced gain degradation in bipolar devices is considered to be the primary threat to linear bipolar circuits operating in the space environment. The damage is primarily caused by charged particles trapped in the Earth's magnetosphere, the solar wind, and cosmic rays. This constant radiation exposure leads to early end-of-life expectancies for many electronic parts. Exposure to ionizing radiation increases the density of oxide and interfacial defects in bipolar oxides leading to an increase in base current in bipolar junction transistors. Radiation-induced excess base current is the primary cause of current gain degradation. Analysis of base current response can enable the measurement of defects generated by radiation exposure.

In addition to radiation, the space environment is also characterized by extreme temperature fluctuations. Temperature, like radiation, also has a very strong impact on base current. Thus, a technique for separating the effects of radiation from thermal effects is necessary in order to accurately measure radiation-induced damage in space.

This thesis focuses on the extraction of radiation damage in lateral PNP bipolar junction transistors and the space environment. It also describes the measurement techniques used and provides a quantitative analysis methodology for separating radiation and thermal effects on the bipolar base current.

To all of my family

ACKNOWLEDGEMENT

I would like to thank my advisor Hugh Barnaby for his support throughout my academic stay at Arizona State University. The enthusiasm we both share for science and mathematics allowed me to learn a world of information while working towards my degree. Connection One provided a wonderful research facility, and took me one step closer to professionalism. I would also like to extend a thank you to the Radiation Effects and Analysis Group (REAG) at Goddard Space Flight Center for their comments, insight, and suggestions while working on my thesis.

TABLE OF CONTENTS

Page

CHAPTER Page

LIST OF FIGURES

Figure Page

LIST OF TABLES

Table Page

1 INTRODUCTION

Semiconductor devices are of great importance to many modern scientific instruments including those that operate in hostile environments. The space environment - home to a great many instruments - is also considered one of the harshest. As the scientific community strives to discover more about the Earth, Sun, solar system, and beyond, the requirements for operation in these inhospitable conditions pushes the limits of semiconductor performance, robustness, and reliability.

Millions of transistors make up the systems that are implemented in space instruments. Therefore, the focus of this thesis is to analyze and model how transistors, specifically bipolar junction transistors, respond to the harsh conditions that the space environment naturally imposes. This harsh environment is primarily characterized by its high level of radiation and extreme temperatures. Analyzing the basic operation and responses of the bipolar device to radiation and temperature extremes enables the development of models that can be used to estimate how transistors and the instruments that use them will perform over the lifetime of a space mission.

Radiation-induced gain degradation is the primary threat to bipolar junction transistors operating in space. Radiation damage to a device may be attributed to several factors; however, the total ionizing dose (TID) accrued after being exposed is one of the dominant causes of device degradation. Radiation-induced excess base current is the primary cause of gain degradation in bipolar transistors. Increased base current is attributed to the buildup of oxide and interfacial defects

in bipolar oxides. Trapped charged in or carrier recombination at these defect sites can cause irregular operation and sometimes failure at the device, circuit, or even system level. To mitigate these deleterious effects, the mechanisms of transistor degradation must be fully understood.

Transistors are the building blocks of more complex electrical systems. As mentioned above, the transistor of interest in this thesis is the bipolar junction transistor (BJT). The particular types of BJTs studied and tested for this thesis are gated lateral PNP bipolar junction transistors. The functionality of these devices and their performance in varied conditions are discussed in detail throughout this document.

BJT response characteristics obtained from experiments in a variety of hostile environments may be affected by a number of external conditions acting at the same time. This work specifically considers the combined impact of ionizing radiation and wide temperature variation on device performance. In order to fully understand the response of a device to these two environmental factors, techniques for "effects separation" must be developed. This document presents models and mathematical methods that capture the independent effects of these two environment variables.

Some BJTs have been shown to exhibit increased sensitivity to the low radiation dose rates characteristic of the space environment. While enhanced low dose rate sensitivity (ELDRS) in BJTs has been demonstrated in ground-based testing, only one space-based demonstration of ELDRS at the transistor level has

been reported. Characterizing ELDRS in BJTs is the primary scientific objective of a new space instrument these test structures are intended to fly on.

Designing an instrument for space flight requires information on the orbit and total expected lifetime. Models of the high energy particle concentrations that instruments will encounter on-orbit provide the necessary information regarding particle fluence for radiation dose calculations. On a spacecraft, the responses of a device to the radiation environment are called space radiation effects.

In chapter 2, this thesis provides a description of the space environment in Earth-orbit. In chapter 3, the basic operation and response of BJTs to the combined impact of radiation and temperature effects is discussed with experimental data provided in chapter 4. In BJTs, the effects of radiation and temperature are strongly coupled, i.e., BJT model parameters are non-linear, inseparable functions of radiation dose and temperature. In order to analyze the effects of radiation on these parameters independent of the wide temperature fluctuations, mathematical functions for these parameters are derived that separate the effects of these two environmental variables. These parameters include, but are not limited to, the base current recombination factor (I_{SE}) and the base current ideality factor (n_e). The derivation of the base current ideality factor's dependence on radiation and temperature is a central component of this manuscript. Detailed analysis and modeling techniques are presented in chapter 5. Ultimately the models allow for radiation damage to the part to be extracted, independent of temperature.

2 SPACE RADIATION EFFECTS

This chapter summarizes the conditions encountered by experiments intended for Earth-orbit missions. However, the general characteristics and behavior of high energy particles in the Earth's magnetosphere are relatable to any space flight mission, whether they be intended for low Earth-orbit (LEO, 300-2000km above earth's surface) or beyond. Information about the basic conditions and characteristics of the space environment is obtained from previous mission data as well as model predictions. The most widely used space radiation models are the AP-8 and AE-8 models that use recorded data over a time-span from 1966 to 1980 [1, 2, 3]. The characteristics of hostile environments vary greatly and must be investigated on a case by case basis. Space has thermal and irradiative variation unlike any ground-based semiconductor application environment. This variation motivates the investigation of bipolar responses in this thesis. For any given space mission, the lifetime of the mission, launch date and orbital trajectory all need to be considered to make a valid estimate of the radiation fluences encountered. This in turn determines the susceptibility and survivability of the electronics on board the spacecraft.

2.1 Environmental Characteristics

The Sun is constantly balancing the force of gravity against the release of energy from nuclear fusion of hydrogen into helium. The release of energy comes in the form of gamma rays and charged particles. The solar activity produces an output of radiation, or solar wind, which directly collides with the Earth's

magnetosphere and alters the trapped particle populations. This interaction is referred to as space weather.

As the force of gravity and fusion churn the composition of the nearest star to Earth, large masses can be ejected from the surface. These are called coronal mass ejections (CMEs). This type of solar activity produces large fluences of protons that can drastically change the near-Earth environment. When CMEs are not directed toward Earth, there is still an integral flux of gamma rays and charged particles (mostly protons) entering the Earth's magnetosphere. The different temporal resolutions of the solar wind activity are referred to as "quiet" and "stormy" conditions. CMEs follow a trend of the Sun's cycle in that they are relatively more frequent during solar maximum. Typically during solar maximum, the Sun's increase in activity leads to stormier conditions at the Earth's magnetosphere. The solar cycle is what makes the launch date crucial for radiation modeling; a mission flown during solar maximum is likely to have a higher dose than if flown with the same trajectory during solar minimum.

The conditions experienced by a spacecraft are also extremely dependant on the inclination of the vehicle's orbit; a more polar orbit (i.e. higher inclination) is more likely to pass through more dense regions of trapped particles whereas an Equatorial LEO mission would need to consider the South Atlantic Anomaly (SAA), both of which are discussed later in this section. Figure 1 illustrates how an orbital inclination is defined, with an inclination of zero degrees being contained in the Equatorial plane.

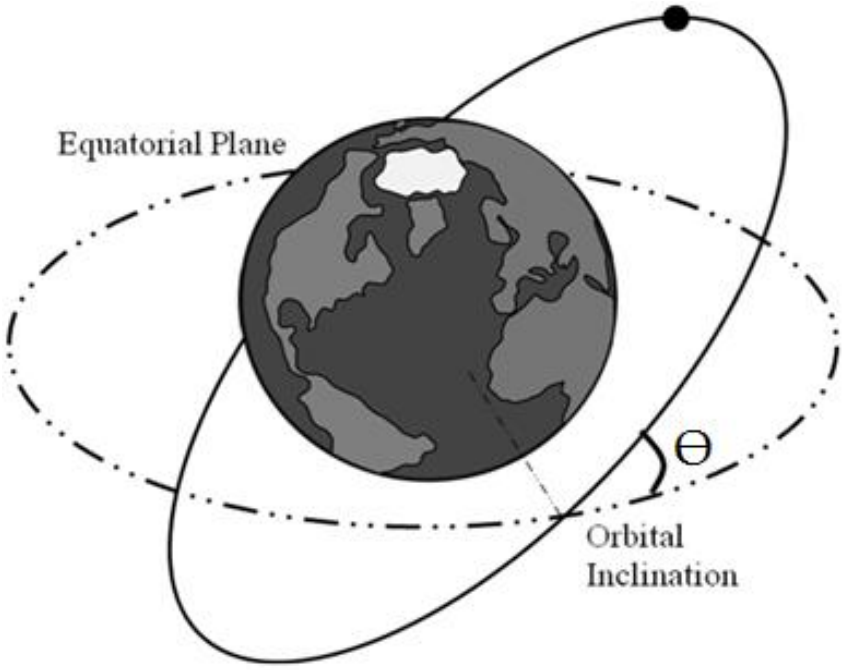

Figure 1: Illustration of orbital inclination angle definition

To show the dependence on inclination, Figure 2 and Figure 3 plot the integral fluences of trapped protons and electrons on two types of orbits both circular with an orbital altitude of 400km. Trapped particles are a primary source of ionizing radiation in LEO. High inclination orbits (i.e., polar) have a much higher fluence of protons than orbits of lower inclination. Thus, at higher inclination, a spacecraft passes through more dense regions of trapped protons. As Figure 3 shows, there is smaller inclination dependence for electrons. For both plots, the points represent the integral fluence of particles that will be greater than or equal to the particle energy listed on the x-axis.

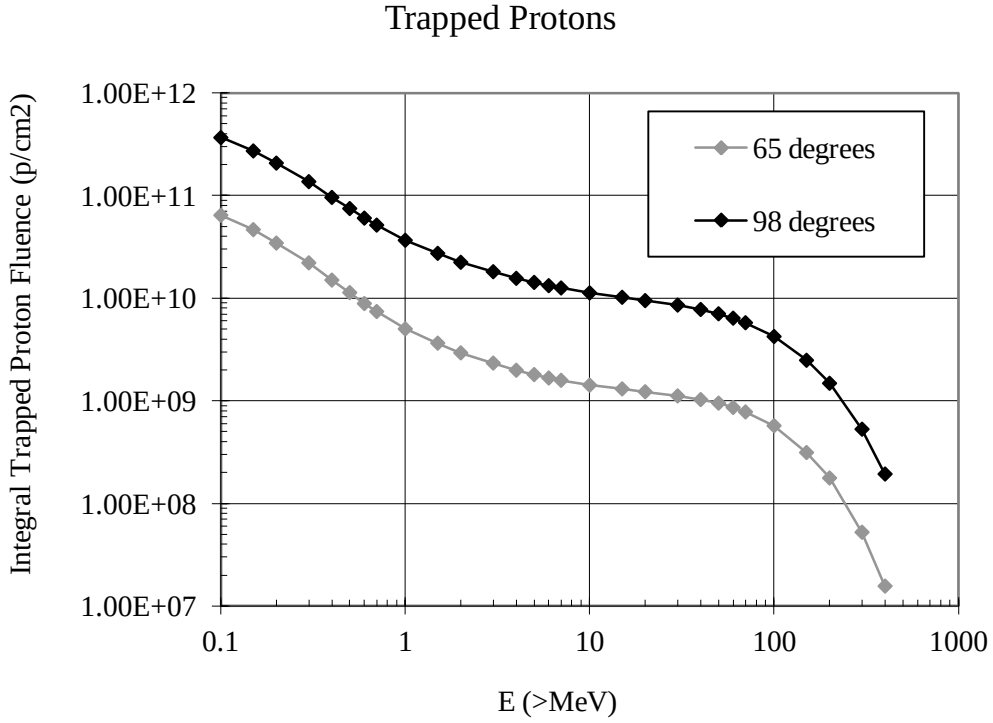

Figure 2: Integral fluence of trapped protons for 65 and 98 degree inclinations

One tool used to evaluate models of the fluence of particles on orbit is SPENVIS, which uses the AP-8 (integral proton) and AE-8 (integral electron) models for solar maximum and minimum, built from spacecraft data taken 1966-1980 [4]. These two models account for the trapped particles present during an averaged solar cycle, but there is always a threat of variation in solar activity that can cause huge deviations from the models [5]. For this reason, it is important to also take into account "stormy" conditions when using the SPENVIS tool for worst case scenario predictions as opposed to "quiet" conditions, as there are higher amounts of radiation due to more solar activity.

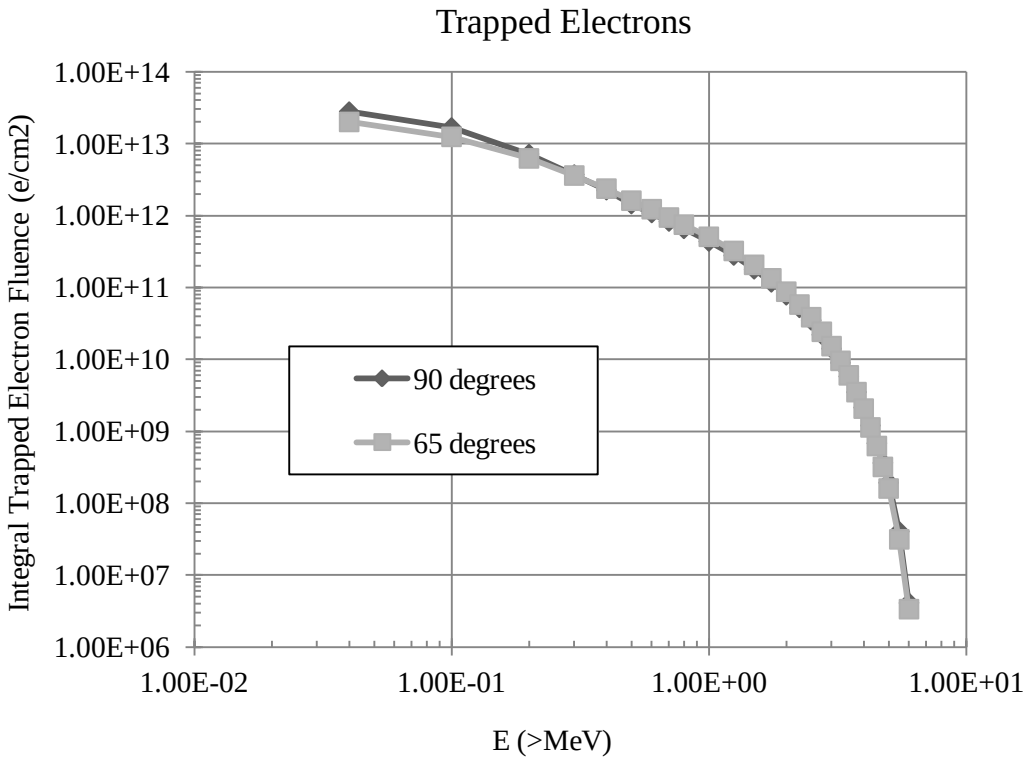

Figure 3: Integral fluence of trapped electrons for 65 and 98 degree inclinations

Knowledge of particle fluences can be used to determine the dose deposited in a component inside a spacecraft if the surrounding materials are known. Figure 4 and Figure 5 both plot the radiation dose for different particles as a function of aluminum shielding thickness over the course of a three year spaceflight mission.

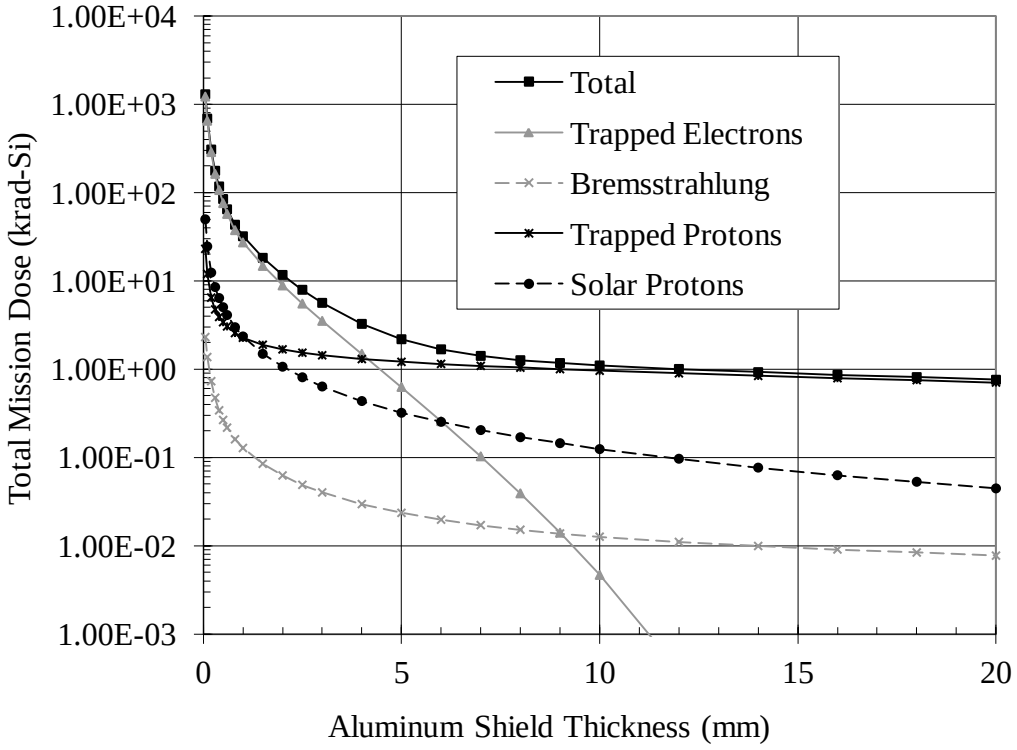

Figure 4: Dose-depth curve over the course of a three year spaceflight mission for a polar orbit, 98 degree inclination at the center of aluminum sphere

Total ionizing dose damage can be caused by the solar protons, trapped protons, trapped electrons, and Bremsstrahlung radiation. Bremsstrahlung or braking radiation is characteristic of electron excitation and photo emission due to an energy transfer from an electron's change in momentum. As the figures indicate, all forms of radiation contribute to the overall total dose exposure. As can be observed in Figure 4 and Figure 5, total dose is strongly dependent on orbital trajectory.

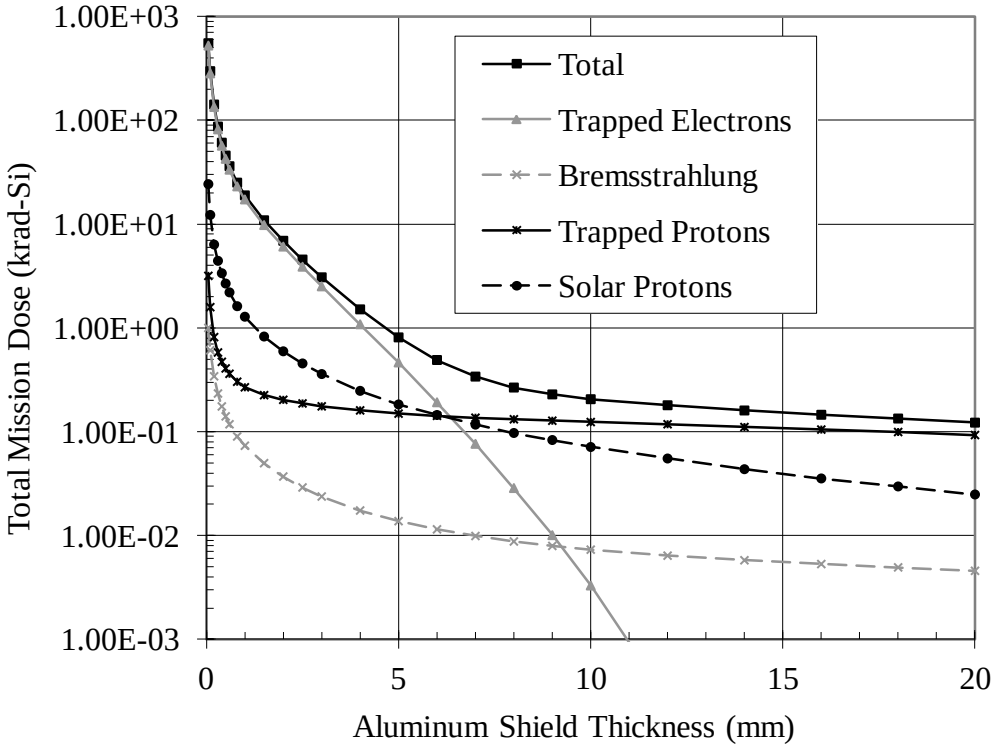

Figure 5: Dose-depth curve over the course of a three year mission for an Earth orbit, 65 degree inclination at the center of aluminum sphere

How these charged particles reside in Earth's magnetosphere depends on the particle energy as well as the natural behavior of charge in a magnetic field. Understanding the shape of the Earth's magnetic field gives insight into the amount of radiation a spacecraft will accrue, and problematic locations.

2.1.1 Space Weather / Trapped Particles

The space environment, primarily Earth-orbit for electronics, is hostile to life forms as well as technology. Extreme fluctuations in temperature and particle distributions are constantly occurring due to the high energy of our nearest star

and the dynamics of the magnetosphere. The Sun periodically releases billions of tons of matter. These immense clouds of material, when directed towards Earth, can cause large magnetic storms in the magnetosphere and the upper atmosphere. The term space weather generally refers to conditions on the Sun and in the solar wind, magnetosphere, ionosphere, and thermosphere [3]. This environment can influence the performance and reliability of both space-borne and ground-based technological systems. In order to fully understand how space radiation impacts the operation of electronics, remote space-based experiments are preferred to ground-based tests. There are several reasons for this preference including:

1. Some space radiation energy is much higher than ground-based sources and thus the efficiencies of spacecraft shielding are better characterized.
2. Proton radiation, one of the most abundant in space, is responsible for both ionization and displacement effects. Ground-based proton testing is both time consuming and expensive.
3. Dose rates in space are difficult to reproduce in ground-based test facilities and may not always provide accurate data (discussed further in Section 2.2.3).

Most of the particle fluences in LEO are well documented [6]. High energy particles are likely to be considered “trapped” in the Earth’s magnetic field. However magnetic sub-storms and solar activity can cause deviations from the effects of just the trapped particles alone. The magnetic field is described as a

dipole in a broad sense but has many parts that are important for understanding space weather. Figure 6 illustrates the magnetic field that protects the Earth's surface and many of its key features. The polar cusps, where the magnetic field lines are closer together, are the regions where some particles can penetrate deepest into the atmosphere resulting in what is known as aurora emissions, or more commonly the northern and southern lights.

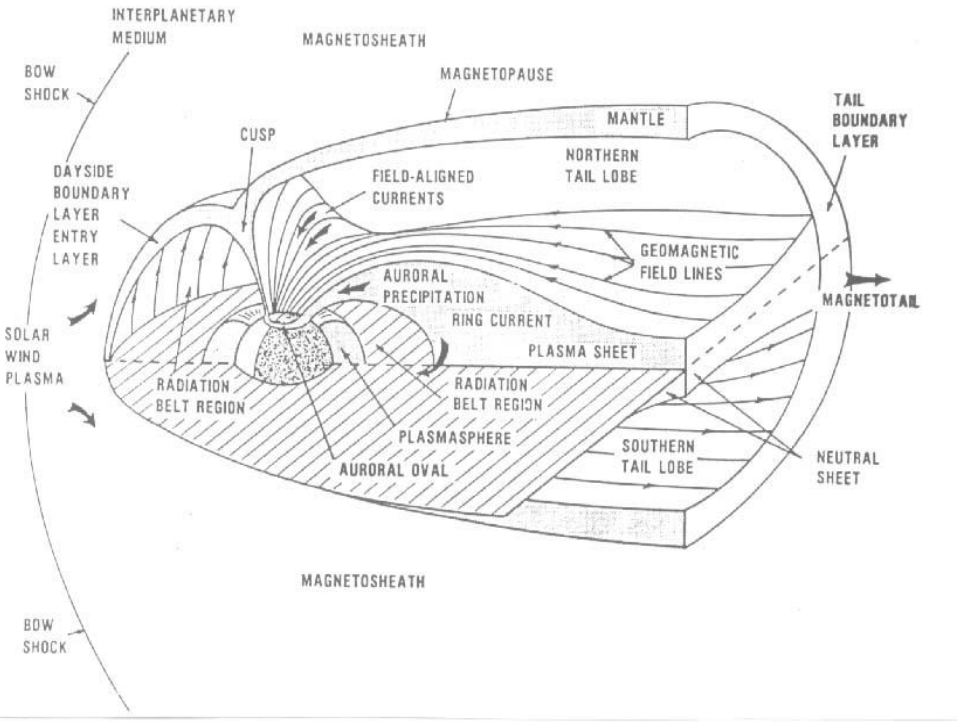

Figure 6: The Earth's magnetic field [6]

The magnetotail has a boundary layer referred to as the magnetopause which dips at the cusp, nearest to the actual magnetic pole. It is important to note that particles beyond this would not become trapped in the Earth's magnetosphere.

However, particles that enter this region do have the potential to interact with the field such that they are drawn closer and sometimes trapped.

2.1.2 Trapped Particles

In a uniform magnetic field, charged particles follow a circular path, due to the Lorentz force,

$$\vec{F} = q\vec{v} \times \vec{B}, \tag{2.1}$$

where q is the magnitude of the charge, v is the charge velocity vector and B is the magnetic field vector. The basic motion is an oscillation called a gyrofrequency; an angular frequency of circular motion in the plane perpendicular to the magnetic field lines. The gyrofrequency is dependent on the mass, m, the charge of the particle, and the magnetic field strength i.e.,

$$\omega_c = \frac{qB}{m}. \tag{2.2}$$

Equation (2.2) is derived from centripetal force offsetting the Lorentz force. If another external force such as gravity in the case of orbital motion is applied, these particles will gyrate with the same frequency and drift in the direction of the additional applied force.

If the magnetic field is non-uniform, as in the case of the Earth's magnetosphere, this changes the gyrofrequency of the charged particle. A stronger magnetic field increases the gyrofrequency and tightens the curl of the particle's path. Under basic assumptions, adiabatic invariants provide insight into the overall motion of particles in a magnetic field.

Three adiabatic invariants are used when describing types of motion that charged particles exhibit in electromagnetic fields. These invariants are not absolute, however, they can be considered constant compared with typical periodicities of the particle's motion. The three invariants are the magnetic moment, μ, for the particle's gyration around the magnetic field, the longitudinal invariant, T, for motion along the magnetic field, and the enclosed magnetic flux, Φ, for the particle's perpendicular drift [3, 6].

From the conservation of energy, the transverse energy and parallel particle energy both have time derivatives that vanish. Adding the two energies together leads to the finding that the magnetic moment does not change. When the particle enters a region of stronger magnetic field it is possible for all of the particle's energy to transport in the transverse direction resulting in what is known as a mirror point. In the case of the Earth's magnetosphere this occurs near the magnetic poles. In a dipole, a particle can bounce from one mirror point to the next, pole to pole, where the magnetic field strength at the mirror point remains the same for like particles with a given energy.

When the particle bounces back and forth in a dipole, this gives rise to a second invariant. Particle drift in the curved magnetic field moves electrons from west to east and protons in the opposite direction. The longitudinal invariant of torque, expressed as

$$T = \oint m v_{\|} ds \text{ [N-m]}, \tag{2.3}$$

can be used to determine the length of the magnetic field lines between two mirror points while undergoing this drift. In Equation (2.3), m is the mass of the particle,

$v_{||}$ is the parallel component of velocity to the magnetic field line, and *ds* is an element of path length over one full oscillation between mirror points. The time of the bounce is on the order of one second, which is considerably greater than the time it takes for one gyration.

The third and final invariance is the total magnetic flux enclosed by the particle's path around the Earth. This invariance is weakly held. However, it provides an insight to the fact that a particle would return to the same field line after making its way around an entire drift shell, i.e. particles of one energy value will not jump from shell to shell.

When the temporal change in the magnetic field surrounding the Earth is much greater than periodicity of these motions, the end result is a grouping of similar particles in toroidal shells that are referred to as radiation belts.

2.1.2.1 The Van Allen Radiation Belts

The trapped particle zones described in the previous section are categorized as the Van Allen Radiation Belts [6]. There are two belts as a result of protons and electrons having different masses. According to the widely used AP-8 models the proton shell has a maximum fluence in the region of L-shells (L representing magnetic field) listed in Table 1. L-shell distance descriptions are typically used when characterizing distance from the Earth's surface [7]. The electron shell (from AE-8) has two local maximum regions again, shown in the table below, with a slot in between where the integral fluence is less. Due to this slot, the variation of electron fluence is extreme in middle Earth-orbits, making

the fluence within the region less predictable. The fluxes listed in the table are long term averages calculated using SPENVIS.

TABLE 1

Trapped Particle Populations

Trapped Particles	L-shell Values	Energies	Fluxes
Protons	L=1.15 to L=10	Up to 100's of MeV	10^5 $cm^{-2}s^{-1}$ (>10 MeV)
Inner Electrons	L=1 to L=2.8	Up to 4.5 MeV	10^6 $cm^{-2}s^{-1}$ (>1 MeV)
Outer Electrons	L=2.8 to L=10	Up to 10 MeV	3×10^6 $cm^{-2}s^{-1}$ (>1 MeV)

Table 1: Trapped particle population description for the Van Allen Belts [6]

Although the belts typically fit into the shells shown above, there is one region where the proton population has a lower altitude with respect to the Earth's surface.

2.1.2.2 South Atlantic Anomaly

The South Atlantic Anomaly (SAA) is a region of abnormally high proton flux centered above the Atlantic coast of Brazil. The SAA is evidence of the asymmetry of Earth's magnetic field. Data shows that the proton flux near the SAA is much higher at lower altitudes than elsewhere around the globe [6]. The

SAA is a threat to spacecraft with orbits having low inclination and low altitude. Figure 7 depicts the offset of true north to magnetic north, which is actually near 11 degrees, and this is why the radiation belts hold an asymmetry.

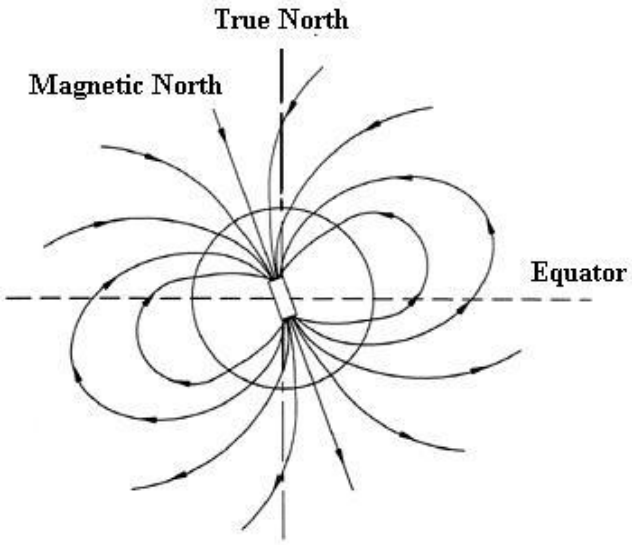

Figure 7: Offset dipole magnetic field of the Earth [6]

The tilt off axis brings charged particles with higher energy to lower altitudes than would be expected. Figure 8 shows a contour of the SAA. As the figure indicates, the size of the SAA is roughly the size of the South American continent.

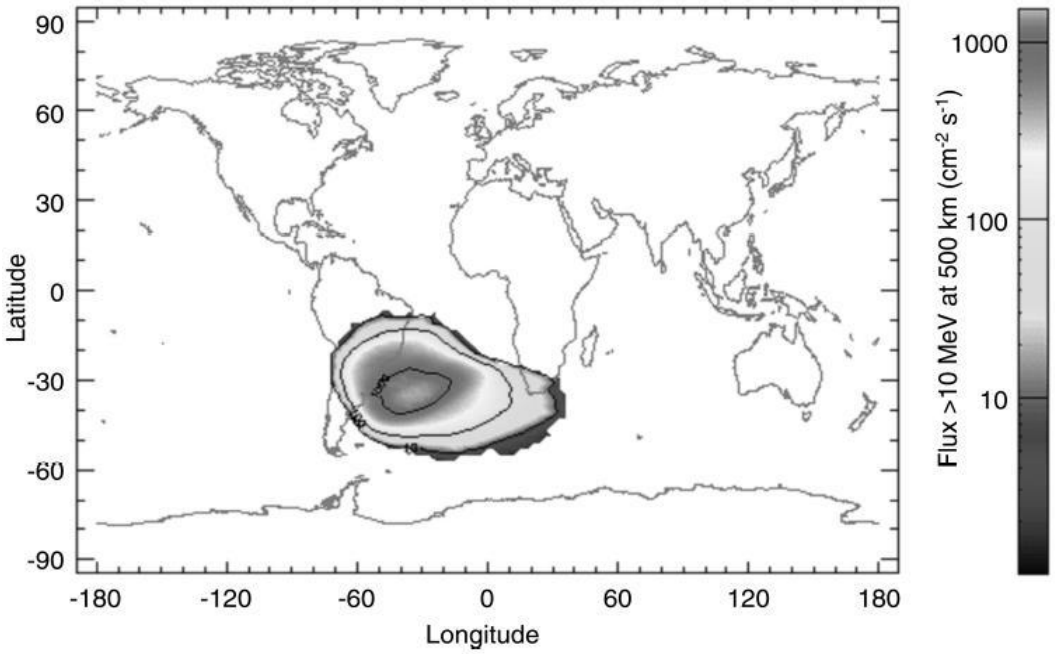

Figure 8: Contour plot of the South Atlantic Anomaly [6]

Understanding these descriptions and the nature of the near Earth environment allow for accurate modeling of the radiation a spacecraft will be exposed to in orbit. This is one variable that an electronic device will encounter, as noted before, it is not the only one.

2.1.3 Temperature Variations

Studies at extreme temperatures are often performed to prove and/or explore the abnormal limits of physical theories on semiconductor materials and devices. However, in the space environment, operation in extreme temperature *is* normal. The profiles of temperatures in Earth-orbit typically range from -15 ˚C to 55 ˚C [8]. Electronic components may self-heat and experience more extreme profiles

without proper mitigation. Understanding the temperature swing during a space mission helps complete the picture of a device response.

2.2 Total Ionizing Dose Effects in Semiconductors

In this section, two basic types of radiation effects are discussed. These are ionization effects (i.e. TID) and displacement damage. Single event effects (SEE) are also important in modern semiconductor devices and ICs but they are not discussed in this thesis [9, 10]. It is important to note that SEEs cannot be ignored when considering risk in a space-based mission.

2.2.1 Incident Radiation

Incident radiation can be single charged particles (e.g. electrons, protons), neutral particles (e.g. neutrons), ionized elements (e.g. Ar, Ne), and high energy electromagnetic waves (e.g. photons, gamma rays, cosmic rays). Bremsstrahlung radiation can also cause ionization through the deceleration of electrons. The braking is governed by Couloumbic interaction between the atoms of the semiconductor lattice or dopants (positively charged) and the oppositely charged particles (electrons). This interaction causes deflection, resulting in a release of energy into the material [11]. These types of interactions and radiation are common in the space environment.

2.2.2 Ionization Effects

Radiation-induced ionization on devices is described by the generation of electron-hole pairs (ehps) within solid state materials. In semiconductor and other

conducting materials (i.e., not insulators), ionization is typically not found to cause permanent damage. Incident radiation can only create ehps if it has a sufficient amount of energy to generate carriers within the material. For silicon, the energy is approximately 3.6 eV. The electron-hole pairs created along the ionizing particle's track in a semiconductor such as silicon spread out before ultimately recombining or being collected at device terminals. However it is not ionization in semiconductors that causes device degradation over time; total ionizing dose (TID) effects are typically attributed to the trapped charge which builds up in dielectric (insulating) layers adjacent to the semiconductor (e.g., in the SiO_2) and traps created at a semiconductor-dielectric interface (such as Si/SiO_2). In a BJT, the base current primarily increases as a result of increased recombination with interface traps [12, 13, 14].

Extracting the amount of trapped charge and interface traps created by radiation is of significant interest when reporting on the radiation damage to a part. The combined bipolar and MOS experiments described by Chen et al. [15] provides measurement methods to extract the oxide trapped charge and the interface trap densities in gated lateral PNP (GLPNP) BJTs. Knowing how many defects have been created can then be related to total dose exposure to the part, and compared over dose rates.

Radiation-induced trapped charge is typically net positive consisting of trapped holes in the oxide layer of the transistors. In some cases electrons may also be trapped near the SiO_2 interface. Once generated in the oxide, some electron-hole pairs will recombine, though many more holes remain due to their

low mobility in the oxide. These holes can then become trapped in the SiO_2 where they contribute to a net positive trapped oxide charge.

Trapped holes at the interface have the ability to trap electrons injected from the semiconductor substrate. It should be noted that this charge is not necessarily permanent, however remains within the part for a fairly long time period, annealing out nearly linearly with log time [14].

Interface traps can be described as energy levels that are introduced within the semiconductor band gap. Donor-like traps, typically assumed to have energies below the intrinsic Fermi energy, hold positive charge at the interface when they donate an electron to the silicon. This occurs when terminal biases fix the Fermi level below the trap energy. Acceptor-like traps with energies above the intrinsic Fermi energy level hold negative charge when they accept an electron from the silicon. This occurs when terminal biases fix the Fermi level above the trap energy. The charge is easily changed when a bias is applied. In a PNP device, interface traps over the base region are predominantly donors. The donors are net positive, and with no bias they add charge much like positive oxide trapped charge [12]. Applying a bias creates an electric field along the interface, where these unintended charges affect the device performance.

The introduction of interface traps also decreases carrier mobility near the surface. For BJTs however, the most important impact of interface traps is that they increase the surface recombination velocity (SRV, *s*) in the base region, providing additional sites for recombination to occur. Surface recombination velocity is proportional to the interface trap density in the BJT and can be

extracted using proper device models, regardless of temperature. This thesis presents how to obtain a valid approximation of SRV and thus estimate interface trap build-up.

2.2.3 Enhanced Low Dose Rate Sensitivity

Historically, most ground-based testing for ionizing radiation response characterization was performed using dose rates greater than 100 rad(Si)/s, which is much greater than the typical rates seen in space. Though these higher dose rates do cause degradation, linear parts exposed at low dose rate typically show an enhancement in radiation sensitivity.

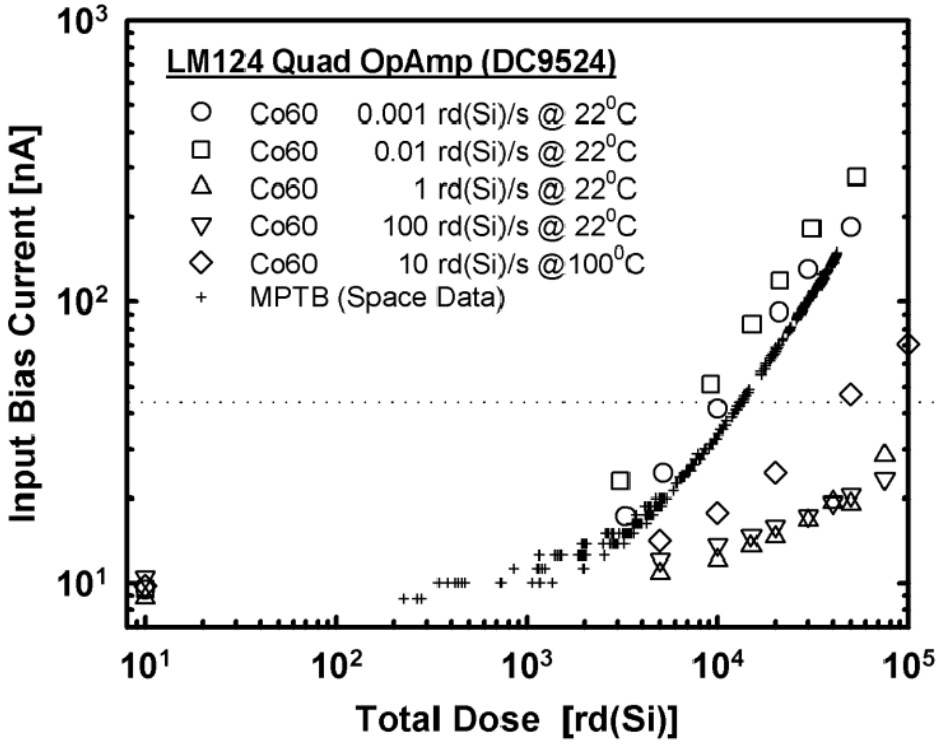

Figure 9: LM124 bipolar device responses according to dose rate for space and ground-based tests [17].

ELDRS in the real space environment was first demonstrated in the Microelectronics and Photons Test Bed (MPTB) program [18, 19]. Figure 9 shows the data taken on an LM124 linear bipolar operational exposed both in space as well as in a ground based laboratory. The ground based tests were performed at different dose rates as well as one elevated temperature. The data show an increase in input bias current (I_{IB}) for the part with increasing total ionizing dose exposure for both the space- and ground-based tests. It also justifies low dose rate testing on the ground. The circuit's I_{IB} is related to the base current for the circuit's input transistor, which are PNP BJTs for the LM124 amplifiers, similar to the devices in this thesis. The data illustrate both the enhancement in degradation at the dose rate is reduced as well as the enhancement in degradation when measured in the lose dose rate space environment. It should also be noted that linear bipolar integrated circuits (operational amplifiers and comparators) fabricated with PNP input devices show a higher damage response to the low dose rate than NPN input parts.

Additional evidence of ELDRS can be found in [16, 17, 18, 19, 20]. As a result of these experiments, ELDRS has been identified as a real, significant effect that impacts the operation of many discrete BJTs and linear bipolar circuits.

2.2.4 Displacement Damage

In addition to TID exposure, BJT operation can be impacted by another radiation effect, displacement damage (DD). Displacement damage is caused by the collision of particles with atoms in a crystalline semiconductor lattice. One tool that is used to statistically understand the basic particle interaction with

materials is Stopping and Range of Ions in Matter (SRIM). As seen in Figure 10, charged particles generally follow a straight path through an example SiO_2/Si (5um/30um) interface if they have enough energy. However, collisions can cause changes in direction, which can be seen as variation from a straight path. The spallation, although slight, can be seen both near the interface and deeper in the bulk material [21, 22].

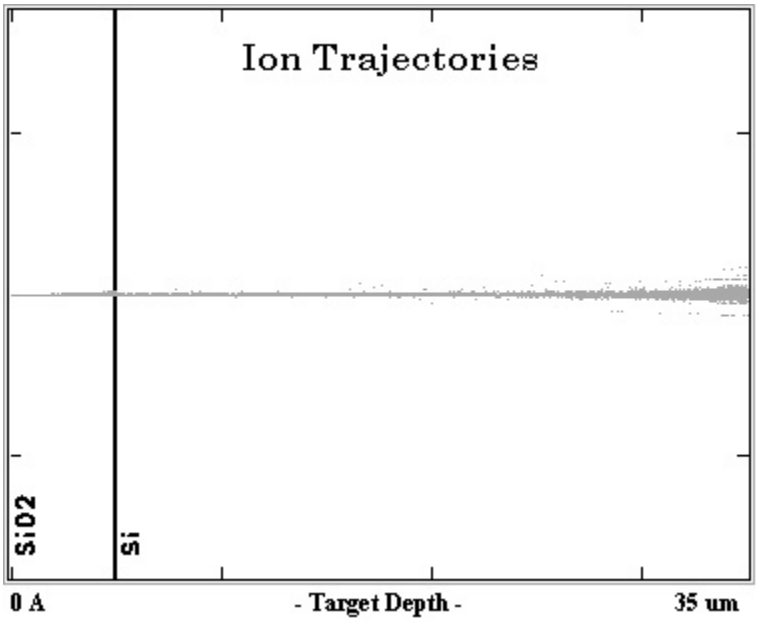

Figure 10: 10 MeV proton trajectories in Silicon and Silicon Dioxide, SRIM output [22]

The atomic nuclei initially displaced by the incident ions are called primary knock-on atoms (PKAs). The damage associated with displaced atoms in the semiconductor lattice is called displacement damage. The amount of DD produced by protons depends on their energy. Protons in space have a wide range of energies, which requires that the DD must be known for the whole range of

proton energies if accurate predictions of total amount of damage are needed. If the incident radiation has enough energy, the PKAs can become a secondary source of radiation, leaving charge deposits again to add to the overall radiation damage in the part [23].

Displacement damage manifests in the bulk of the device, where the silicon lattice is required to be uniform. The parameter that changes due to DD is the carrier lifetime (τ) for the bulk material. Damage to the bulk of the device creates more generation centers degrading the gain of the device by taking away minority carriers, inducing a leakage current. While this does affect the overall device response, it does not primarily change the base current of the device much like TID. Displacement damage is not the focus of this thesis because our aim is to separate thermal and radiation effects from the base current.

3 BIPOLAR JUNCTION TRANSISTORS IN SPACE ENVIRONMENTS

Semiconductor devices employed in the space environment experience wide temperature fluctuations over the course of the mission, e.g., on a typical satellite, the operational temperatures range from -15°C to 55°C [8].

In addition, radiation from the Sun, cosmic rays, and trapped particles, continuously bombards these devices. In order to understand and characterize how semiconductors and associated circuitry respond to these hostile conditions, ground-based and if possible spaceflight tests are performed. Analyzing device response to temperature variability and radiation damage independently is critical to understanding the impact of the space environment on flight parts. However, as shall be discussed in subsequent chapters, separating the effects of temperature and radiation can prove to be a difficult task. This difficulty can be overcome with an in-depth understanding of the device physics and parametric dependencies on both total ionizing dose and temperature.

3.1 Bipolar Junction Transistors

Bipolar junction transistors (BJTs) are comprised of two back-to-back p-n junctions, a collector (C) to base (B) junction and an emitter (E) to base junction. The base region, shown as the n-type region in Figure 11(a) for a representative PNP BJT, is engineered to be much shorter than the typical diffusion length for the minority carriers. This enables the current-voltage relationships for both junctions to be coupled to each other [24].

In a forward active configuration, the emitter-base junction is forward biased ($V_{eb} > 0$V) and collector-base junction is reversed biased ($V_{cb} \leq 0$V). Figure 11(b) shows the sign conventions for the PNP BJT with active bias current flow referenced in the positive direction. For a typical BJT biased in the active mode, the base current (I_B) is smaller than the collector current (I_C) by a current gain factor of β, which makes the BJT a current amplifier [24, 25]. The parameter β is called the common emitter gain. Ionizing radiation damage in BJTs is primarily characterized by an increase the base current for a fixed collector current, i.e., reduced current gain. This increase in base current is due to the build-up of defects in the bipolar base oxide [26, 27, 28]. While it is possible for some of these defects to be removed or compensated by annealing processes, many of the defects remain fixed in the oxide material, leading to permanent damage to the bipolar device. Temperature variability can also cause currents to vary in BJTs and in some cases lead to changes in the current gain. However, these fluctuations are generally not permanent.

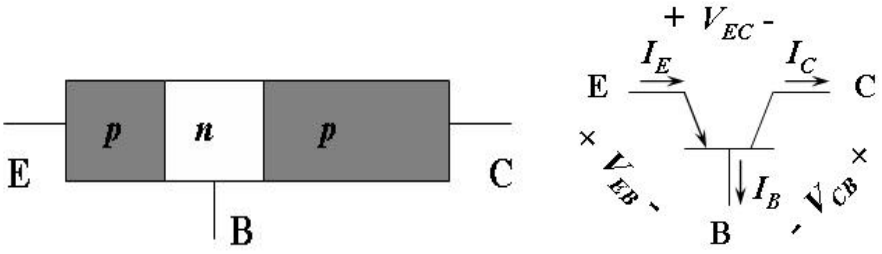

(a) (b)

Figure 11: (a) Emitter, base, collector (b) sign conventions for a PNP-type BJT [29]

The devices tested and analyzed in this thesis are lateral PNP BJTs. Lateral PNP BJTs have been shown to be the bipolar device most susceptible to ionizing radiation damage [30]. The experimental devices were fabricated on specialized test chips in National Semiconductor's linear bipolar process. The test chip, shown in Figure 12 (a), comprises 3 lateral PNP BJTs and well as a standard vertical NPN device. The NPN BJT was included on the chip for process and temperature monitoring. Two of the three lateral PNP BJTs have gate metallization deposited above the active gate region. The layout of these gate controlled lateral PNP (GCLPNP) BJTs is shown in Figure 12 (b). The efficacy of the gate for radiation effects characterization in BJTs has been well documented [12, 27]. Gate control has also been suggested as one methodology for mitigating radiation effects in BJTs. Gated lateral PNPs mitigate radiation effects by using this gate to reduce the depletion region width such that the radiation-induced recombination current is reduced [31,32].

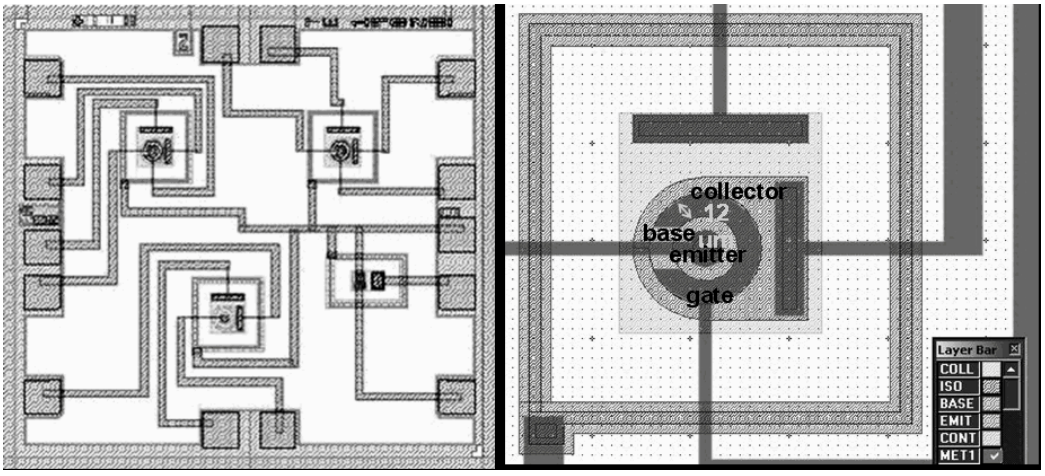

Figure 12: (a) GCLPNP chip, (b) Lateral PNP layout detail [16]

3.1.1 Ideal operation

For a PNP BJT in ideal forward active operation, the forward-biased emitter-base junction injects holes from the emitter. The injected holes diffuse across the short base and are subsequently swept into the collector via the high field across the reversed biased collector-base junction. Hole flux into the collector determines the collector current. Base current in a PNP BJT is ideally determined by the flux of electrons "back-injected" from the base into the emitter. High common emitter current gain is achieved when the ratio of hole flux into the collector is much greater than the flux of back-injected electrons into the emitter. Ideally, both the base and collector current components are characterized as minority carrier diffusion currents.

3.1.2 Non-Ideal operation

Non-ideal operation in a PNP BJT is characterized by not only the ideal base and collector currents described above, but also additional currents associated with carrier recombination in the emitter-base junction and within the neutral base. It should be noted that there are other non-ideal current components, e.g., electron transport across the reversed biased collector-base junction and high injection currents (Kirk, Rittner, etc.). This thesis will only consider one (ideal) component of collector current and three base current components: ideal emitter "back-injection", neutral base recombination current, and emitter-base depletion region recombination current. Particular attention will be paid to emitter-base

depletion region recombination current as it is the primary mechanism for increased base current in BJTs exposed to ionizing radiation [26, 33].

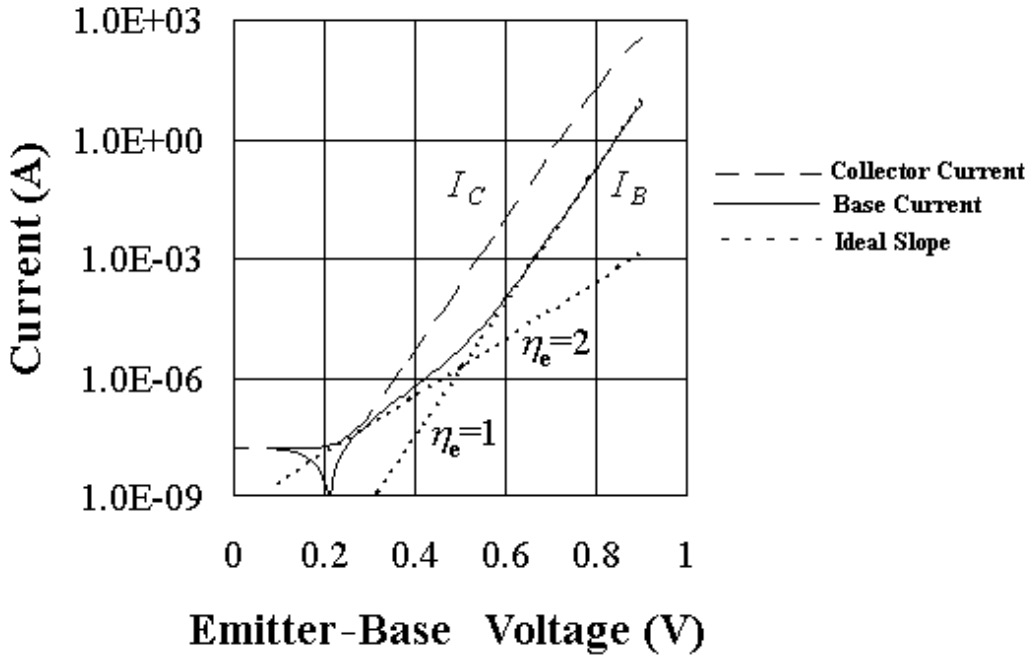

Figure 13: Ideal Gummel curves for a BJT [34]

Figure 13 plots the characteristic base and collector responses as a function of emitter-base voltage (V_{eb}) for a PNP BJT operating in its forward active mode. As the figure shows, the log of the collector current between 0.3V and 0.8 V varies linearly with V_{eb} and can be modeled as

$$\begin{aligned} \ln(I_C) &= \ln\left(I_S \exp\left(q\frac{V_{eb}}{n_f kT} \right) \right) \\ &= \ln(I_S) + q\frac{V_{eb}}{n_f kT} \end{aligned} \quad . \qquad (3.1)$$

In Equation (3.1), the parameter I_S is the saturation current parameter and n_f is the forward emission coefficient (or ideality factor). Figure 13 also shows that the log of the base current in this same voltage range. The base current can be modeled as the sum of two linear equations

$$I_b = \frac{I_S}{\beta}\exp\left(q\frac{V_{eb}}{n_f kT}\right) + I_{SE}\exp\left(q\frac{V_{eb}}{n_e kT}\right) = I_{b,ideal} + I_{reb} \quad . \quad (3.2)$$

In Equation (3.2), the parameter β is the forward current gain factor, I_{SE} is the base-emitter leakage saturation current, and n_e is the base-emitter leakage coefficient (or low-injection ideality factor). Equations (3.1) and (3.2) are the standard DC equations for forward active operation in the Gummel-Poon (GP) model for BJTs. For emitter-base voltages between 0.6V and 0.8 V, the collector and base currents are roughly parallel on a logarithmic scale and the difference in these curves is representative of the forward current gain factor. The second summand (I_{reb}) in Equation (3.2) is the low injection characteristic. For biases below 0.6V, this component may begin to dominate the base current response. This thesis aims to take advantage of this response and separate it from temperature effects.

As will be discussed in later chapters, this non-ideal component of base current increases substantially as a function of radiation exposure and is key to the characterization of radiation effects in bipolar technologies. In detail, this component of the base current will be shown to be dependent on recombination in the depletion region as well as at the surface. Two device parameters that describe

this recombination are the recombination lifetime of the bulk material, τ, and surface recombination velocity, s. More detailed analyses of the forward active collector and base current models and there parameters are given in the next section.

3.1.3 Gummel-Poon Model Parameters

Ideally, the saturation current parameter due to drift can be expressed as

$$I_S = A_E \frac{qD_p n_i^2}{N_D w_B} \tag{3.3}$$

where q is the magnitude of electronic charge, D_p is the diffusion constant for holes, N_D is the donor doping concentration of the base (assumed uniform), w_B is the base width, n_i is the intrinsic carrier concentration for silicon, and A_E is the cross section area of the active emitter-base junction. This is what dominates the collector current.

The forward gain factor, β, is equal to the ratio of collector current to the sum of the "back-injected" ($I_{b,ideal}$) and recombination (I_{reb}) components of base-current (see Equation (3.2)). Since drift dominates the collector current, the forward gain factor can be expressed as

$$\beta = \frac{I_{c,ideal}}{I_{b,ideal} + I_{reb}} = \frac{A_E \frac{qD_p n_i^2}{N_D w_B}}{A_E \frac{qD_n n_i^2}{N_A w_E} + \left(A_E \frac{qn_i^2 w_B}{2N_D \tau} + P_E \frac{qn_i^2 w_B s}{2N_D} \right)}, \tag{3.4}$$

where D_n is the diffusion constant for electrons, N_A is the acceptor doping concentration of the emitter (assumed uniform), w_E is the emitter width, P_E is the

perimeter of the active emitter-base junction, τ is the bulk carrier lifetime, and s, seen again, is the recombination velocity for carriers at the base-oxide interface. This accounts for recombination in the bulk of the device as well as along the surface. The base and emitter widths can be obtained from the device layout. For the devices considered here, w_B = 12 µm and w_E < 1µm. As indicated in the equations above, along with the thermal voltage (kT/q), the parameter n_f determines the log-linear slope of both collector current and the sum of $I_{b,ideal}$ and I_{reb}, or base current, in Figure 13. The default value of n_f in the Gummel-Poon model is one.

The parameter I_{SE} (Equation (3.2)) in the base current's non-ideal emitter-base depletion region recombination component (I_{reb}) is typically expressed as

$$I_{SE} = A_E \frac{qn_i}{2w_d\tau} + P_E \frac{qn_i s}{2w_d}, \tag{3.5}$$

where w_d is an appropriate fraction of the emitter-base depletion region. In this model, the thermal voltage and the parameter n_e determine the log-linear slope of I_{reb} with respect to V_{be}.

It can be observed in Equations (3.1) and (3.2), that temperature, through its effect on thermal voltage, impacts both the collector and base current slopes. Temperature also impacts the model parameters I_S, β, and I_{SE} above by altering the diffusion constants and intrinsic carrier concentrations.

Extreme temperatures can also impact the ionized doping concentrations, however this type of temperature variability will not be considered here. The

doping concentrations, N_D and N_A, are taken from the doping profiles shown in Figure 14, i.e., $N_D \sim 10^{18}$ cm^{-2} and $N_A \sim 10^{15}$ cm^{-2}.

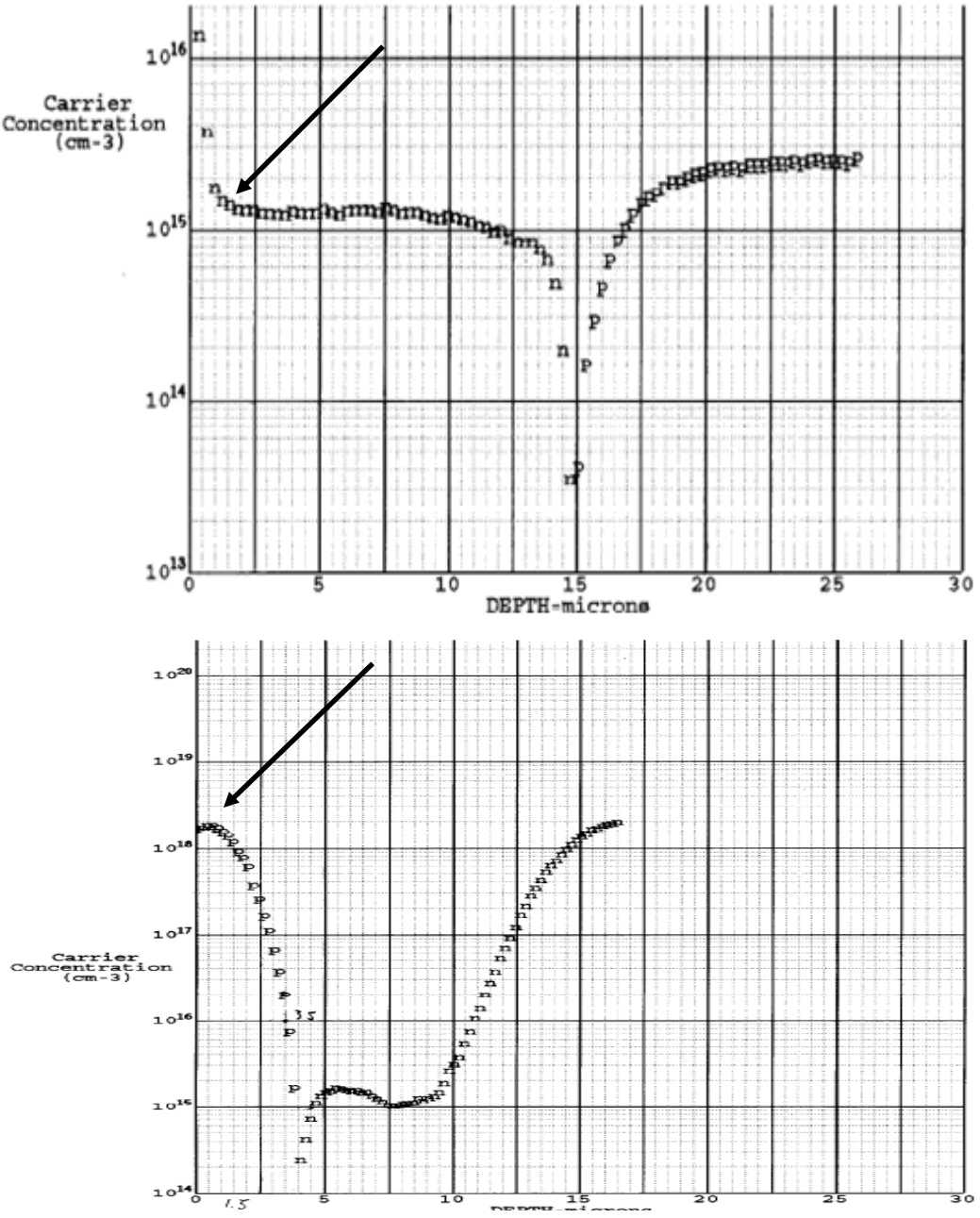

Figure 14: Doping profiles for the lateral PNP-type BJT obtained from spreading resistance measurements (taken vertically down through the base and emitter respectively), arrows depict the value of donor/acceptor at the p-n junction.

The non-ideal ideality factor, $n_{e,}$ is of considerable interest and is investigated as a quantity dependant on many other device parameters. The ideal value of 2 is commonly used. The significance of n_e as well as I_{SE} comes into play when dealing with radiation-induced degradation.

3.2 Radiation Effects and Thermal Implications

Increasing total dose and temperature both increase the base current. This similarity can cause a misinterpretation of data. In order to characterize device degradation with radiation, it is important to extract the impact of thermal effects.

Mathematical models can enable the separation of radiation and thermal responses. Once the mathematical model is derived, the effects of temperature and radiation can be isolated and characterized. For the purposes of this thesis, the focus will be on the non-ideal base current component and its sensitivity to temperature and radiation.

Indeed, radiation-induced alterations in both n_e and s in Equations (3.2) and (3.5) are critical factors that determine ionizing damage in BJTs. It will be shown that the simple formulation in Equation (3.5) does not fully capture the physics of base current in low injection, particularly when radiation and temperature effects are both considered. A more detailed equation will be derived which will more accurately model the combined effects of radiation and temperature on I_{reb} and enable independent analysis of these two environmental variables on base current and current gain in PNP BJTs.

4 TEST METHODS AND EXPERIMENTAL DATA

In this chapter, the test methods used for obtaining experimental data are discussed. Data from measurements on one device are reported and used to illustrate new techniques for analyzing and characterizing BJT response to both radiation damage and temperature variation.

4.1 Ground-Based Testing

In order to characterize (or experimentally simulate) how semiconductor devices will respond in hostile environments (i.e. radiation and extreme temperature environments), ground based testing must be performed. With a ground based test, the effects of total dose and temperature on devices can be characterized and analyzed separately. Since a primary, first order effect of increased total dose and temperature is an alteration in collector and base current while the device is in active mode, the BJT test method consists of monitoring base and collector current while the collector-base junction is reversed biased and the emitter-base junction is forward biased (Gummel curves). For PNP BJTs, a typical bias scheme sets the base terminal to ground, the collector voltage to -1V (in order to ensure operation in active mode), and the emitter voltage is swept between 0V and 0.8V. Gummel curves are plots of the log collector and log base currents vs. base-emitter voltage [35, 36, 37]. The use of a log-linear plot allows for analysis of base current at lower current levels [33, 38]. All test results reported in this thesis are obtained with this test method. The test setup is illustrated in Figure 15 below. An Agilent 4156 parameter analyzer is used to set

the biases and run the desired sweep while reading out the appropriate currents. The 4156 was used for both radiation and temperature testing.

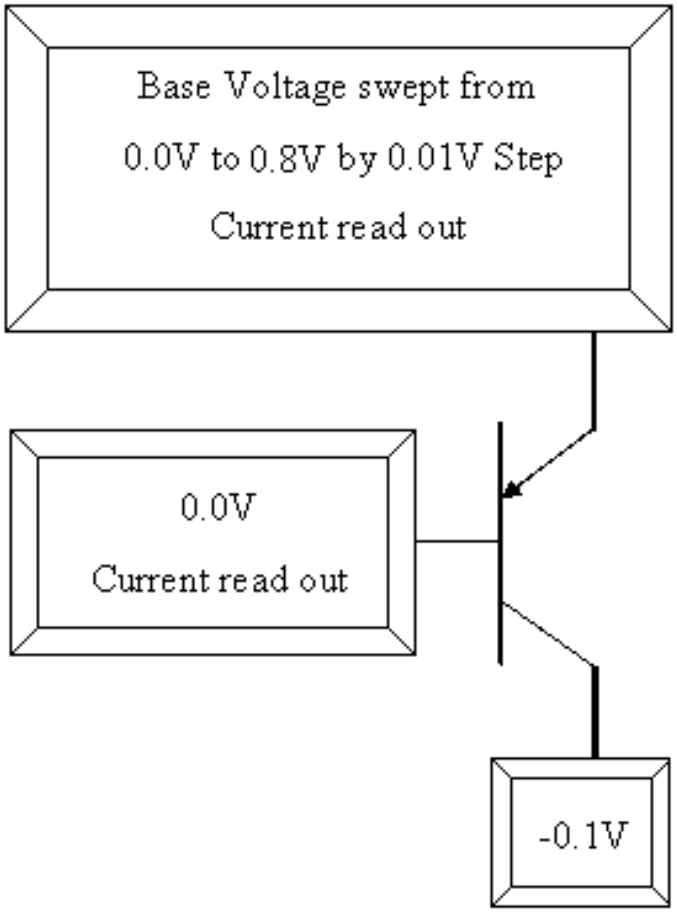

Figure 15: Gummel test setup, emitter and base current collection

4.2 Irradiation Test Results

Radiation testing was performed at Arizona State University (ASU) with a Gammacell 220, Co^{60} gamma ray source. To achieve a final TID of 300 krad(Si), the chips were step stressed to levels of 30 krad, 100 krad, and 300 krad, with data taken at room temperature after each step. While being irradiated, the devices

were grounded on all terminals. The resulting Gummel curves are shown in Figure 16.

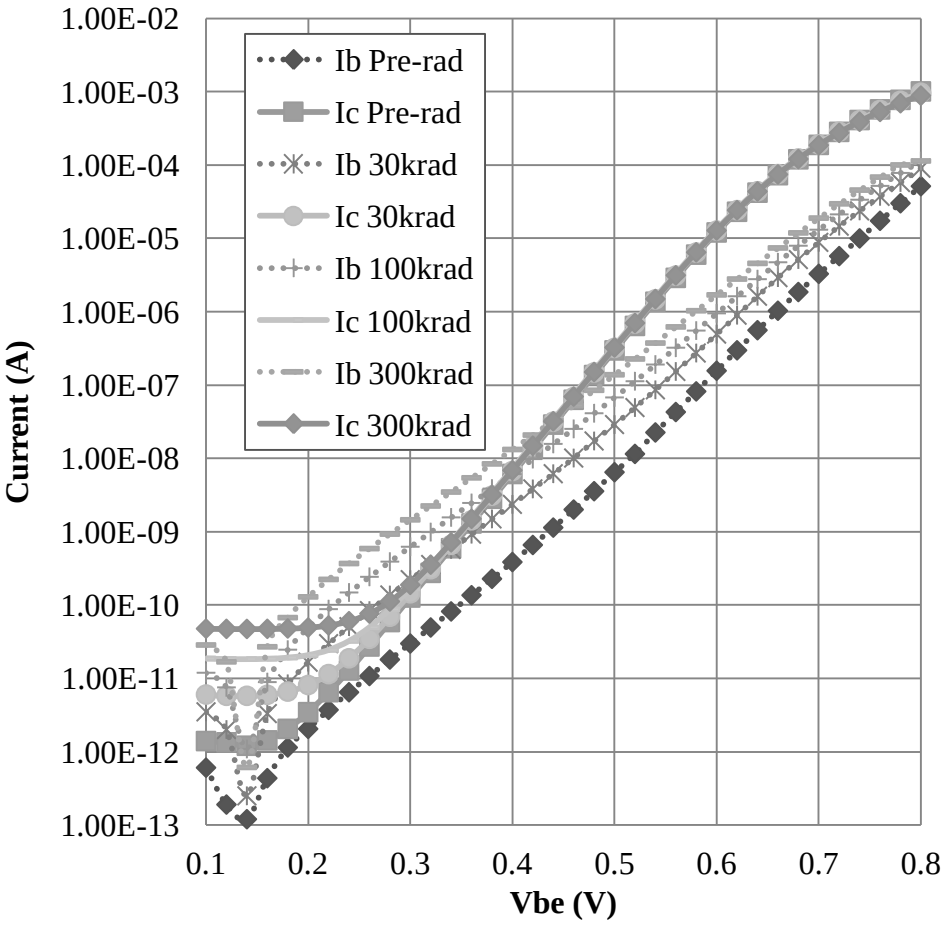

Figure 16: BJT currents vs. emitter-base voltage pre- and post-irradiation

In order to irradiate multiple chips simultaneously while ensuring identical levels of dose on each chip, parts were placed in the radiation chamber so as to lie on the same isodose lines. The isodose curves for the Gammacell 220, provided by Atomic Energy of Canada Limited [39], are shown in Figure 17.

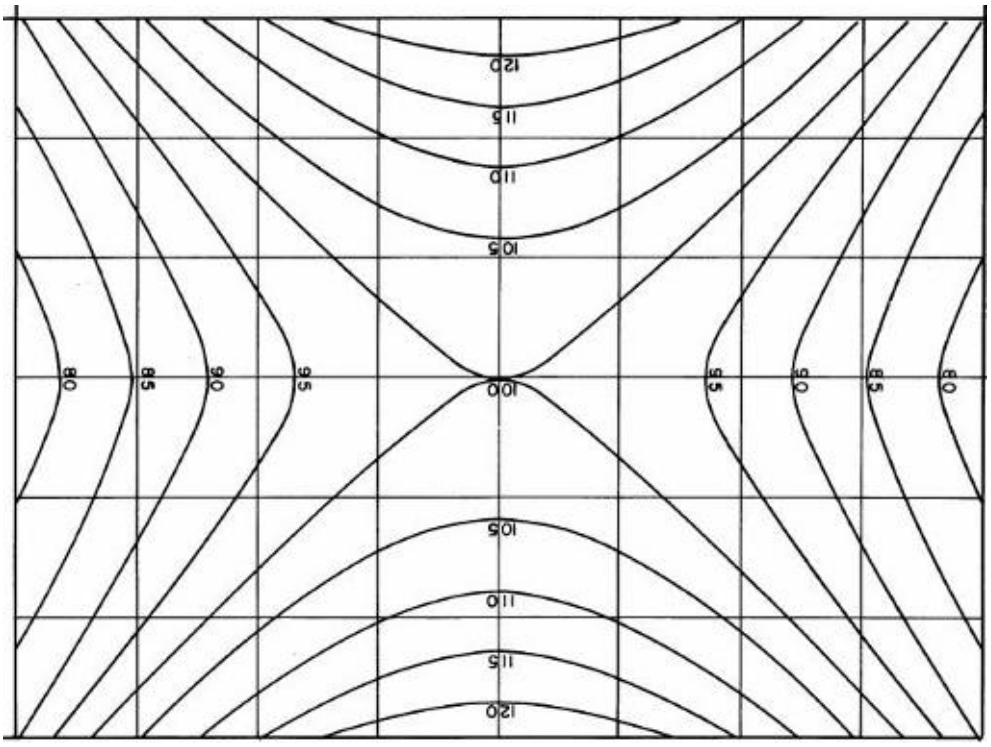

Figure 17: Isodose curves for the Gammacell 220 radiation chamber [39]

4.3 Temperature Test Details

Temperature tests were conducted on un-irradiated and exposed parts to characterize thermal variation as a function of dose and to validate models. The thermal chamber used in these experiments has an internal thermocouple which was used to automatically stabilize the ambient temperature near the chips during testing. A second stand alone thermocouple was placed inside the chamber below the test chip package (see Figure 18) to confirm the temperature of the parts during testing.

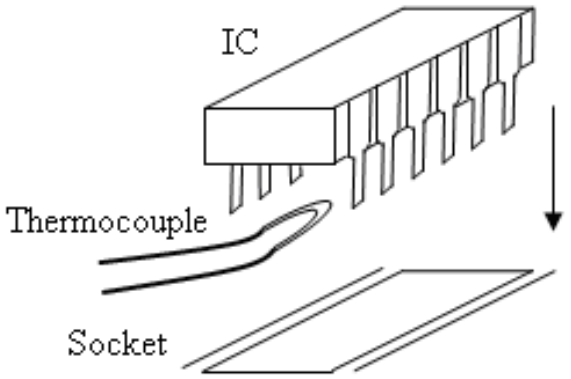

Figure 18: Thermocouple location during temperature testing

Temperature response testing was performed at the following temperatures: -30 ˚C, 0 ˚C, 30 ˚C, 60 ˚C and 90 ˚C. Appropriate settling times were chosen (i.e., on the order of 15 minutes after initial temperature setting) in order to ensure thermal equilibrium during measurement.

Figure 19 plots the current vs. emitter-base voltages for various temperatures for the un-irradiated parts. The base and collector currents are shown on separate plots for clarity as they tend to overlap with increasing temperature. Figure 20 plots the results after 300krad of total dose.

4.3.1 Pre-Radiation

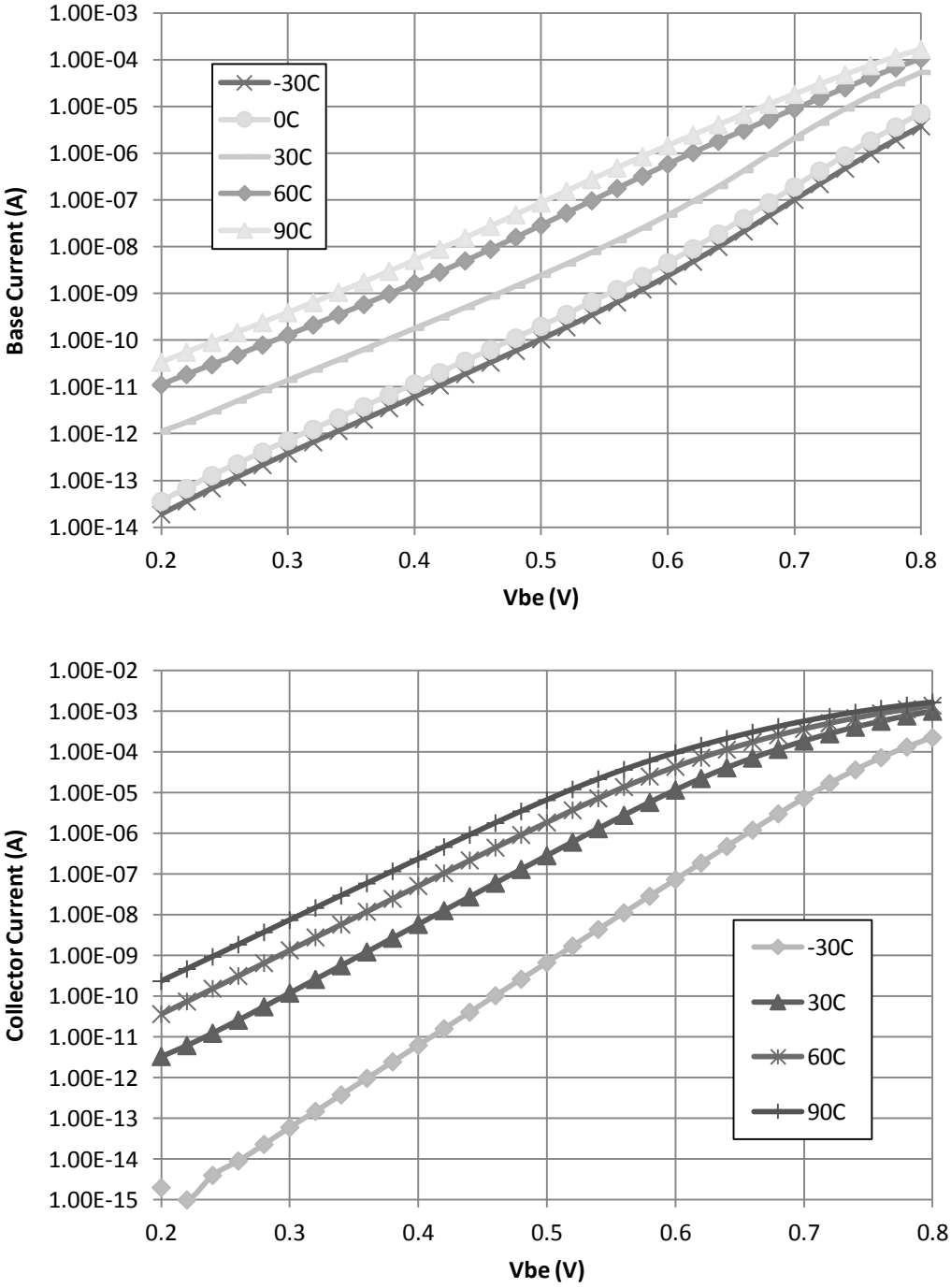

Figure 19: BJT currents for various operating temperatures pre-rad

4.3.2 Post-Radiation

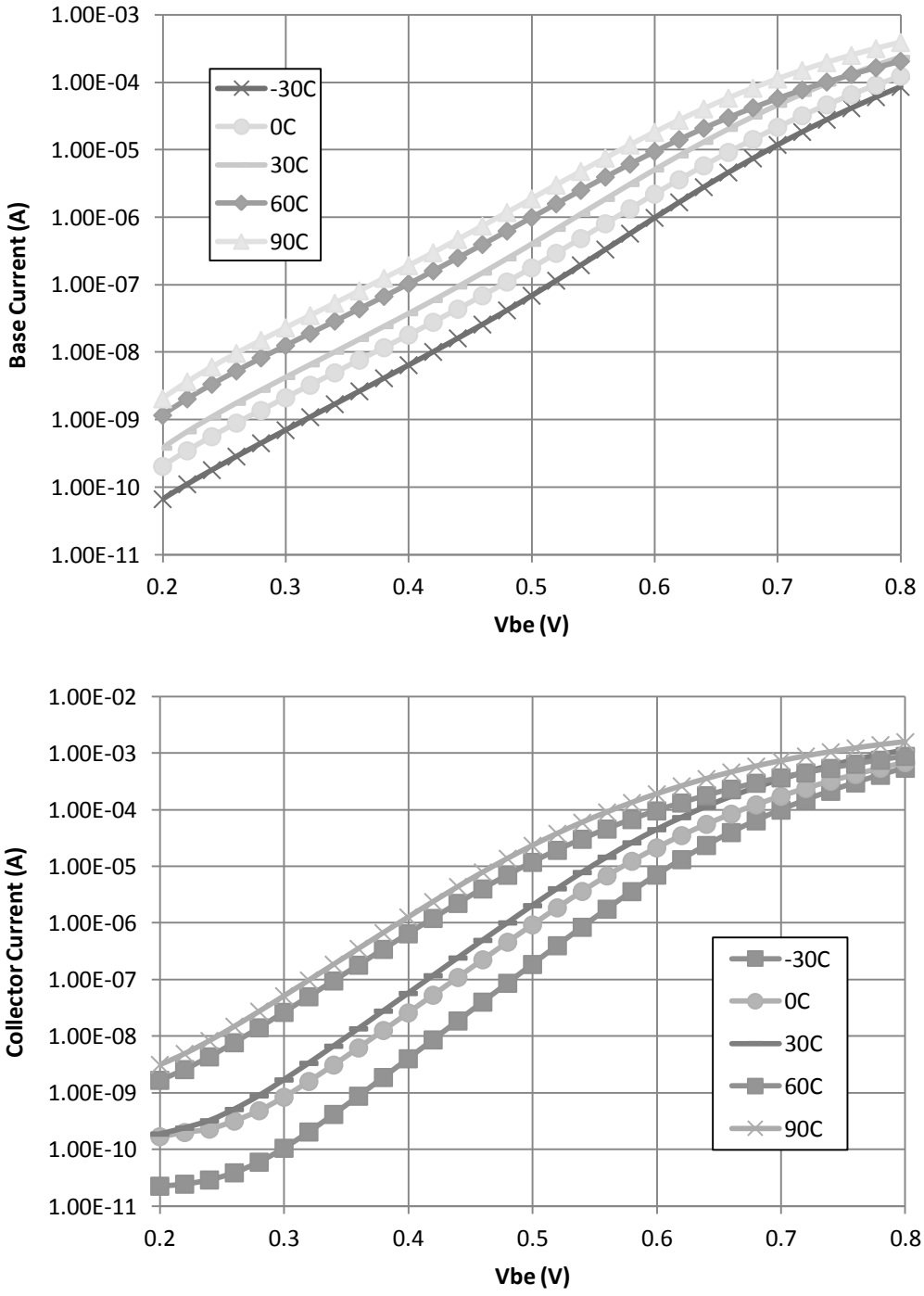

Figure 20: BJT currents for varied operating temperatures post-rad (300k)

The results in these figures show that there is a similar response from the gated lateral PNP transistors to radiation and temperature, in that the base current increases with dose as well as temperature. Collector current is shown to depend on temperature and radiation, more so by temperature. As will be discussed in the following section, in order to separate these effects, accurate models must be derived.

5 MODELING AND ANALYSIS

This chapter presents a modeling technique that separates the combined effects of temperature and radiation so that both effects may be analyzed independently.

While mathematical models describing the effects of radiation on bipolar junction transistors have been presented in previous studies [30, 40], none of the models have included the impact of temperature variation on device radiation response, particularly on the base current characteristics. In this chapter a mathematical model that accurately captures the dependence of base current on both temperature and radiation damage is derived and validated with ground-based test results.

5.1 Temperature Models for Base Current

The impact of temperature on $I_{b,ideal}$, I_{reb}, are fairly well understood. However temperature effects on base currents at low injection, i.e., currents due to depletion region recombination, are much less understood. Since degradation in the low-injection base current (I_{reb}) is the component that primarily increases with TID exposure [35, 38], accurate modeling of temperature effects in this region of operation is critical.

With respect to ideal base current ($I_{b,ideal}$), thermal effects are primarily captured by three parameters: the intrinsic carrier concentration (n_i), the electron diffusion constant (D_n), and the thermal voltage (kT/q). Common material parameters that impact n_i and D_n are listed in Table 2, with their room temperature

values reported. Base current due to neutral base recombination (I_{rb}) is also a function of n_i. However, since the contribution of I_{rb} is typically much smaller than $I_{b,ideal}$ across the temperature range of interest, its effect will be neglected. It should be noted that ionizing radiation, through its impact on surface recombination velocity (s) can impact I_{rb} as well. However, previous studies have shown the impact of I_{rb} to be small relative to the contribution of space-charge recombination current (I_{reb}) in irradiated BJTs [41].

TABLE 2

Constants used and Common Device Parameters at 303K

Constant or Parameter, symbol	Value [Units]
Intrinsic Carrier Concentration, n_i	10^{10} ·[1/cm^3]
Effective electron mass, m_e	$1.08\text{x}10^{-30}$ ·[kg]
Effective hole mass, m_h	$0.74\text{x}10^{-30}$ ·[kg]
Electron mass, m_o	$9.11\text{x}10^{-31}$ ·[kg]
Band Gap Energy, E_g	1.125 ·[eV]
Electron Mobility, μ	1300 ·[cm^2/V·s]

Table 2: Constants and Values recorded in silicon [25, 42]

5.1.1 Intrinsic Carrier Concentration

The dependence of n_i on temperature can be expressed as [42],

$$n_i = \left(N_c N_v\right)^{1/2} \cdot \exp\left(\frac{-E_g}{2kT}\right), \tag{5.1}$$

where E_g is the energy band gap for the semiconductor material. The band gap is dependent on temperature itself and can be modeled by the empirical relationship [42]:

$$E_g(T) = E_g(0) - \frac{\alpha T^2}{(T+\beta)} \tag{5.2}$$

In Equation (5.2), $E_g(0)$ is the limiting band gap at zero Kelvin and assumed equal to $E_g(0) = 1.170\,\text{eV}$. The values for α and β are 4.47x10^{-4} eV/K and 636 K, respectively.

N_c and N_v in Equation (5.1) are effective density of states in the conduction and valence band, respectively. These parameters are dependent on temperature as shown in the following equations (derived from Maxwell-Boltzmann approximation):

$$N_c = 2\left(\frac{m_h kT}{2\pi\hbar^2}\right)^{3/2} \tag{5.3}$$

$$N_v = 2\left(\frac{m_e kT}{2\pi\hbar^2}\right)^{3/2} \tag{5.4}$$

In Equations (5.3) and (5.4), $\hbar$ is Planck's constant, m_e is the effective mass of the electron, and m_h is the effective mass of a hole. The two effective masses are also dependent on temperature as shown in the following empirical equations:

$$\frac{m_h(T)}{m_o} = 1.028 + T \cdot (6.11 \times 10^{-4}) - T^2 \cdot (3.09 \times 10^{-7}) \quad , (5.5)$$

$$\frac{m_e(T)}{m_o} = 0.61 + T \cdot (7.83 \times 10^{-4}) - T^2 \cdot (4.46 \times 10^{-7}) \quad . (5.6)$$

Finally, the intrinsic carrier concentrations dependence on temperature can be expressed as

$$n_i(T) = \sqrt{\frac{m_h(T)^{3/2} \cdot m_e(T)^{3/2}}{2}} \left(\frac{kT}{\pi \hbar^2} \right)^{3/2} \cdot \exp\left(\frac{-E_g(T)}{2kT} \right) . (5.7)$$

The variation of n_i with temperature can be seen in Figure 21, which shows an increase over an order of magnitude over a range of about 50 degrees.

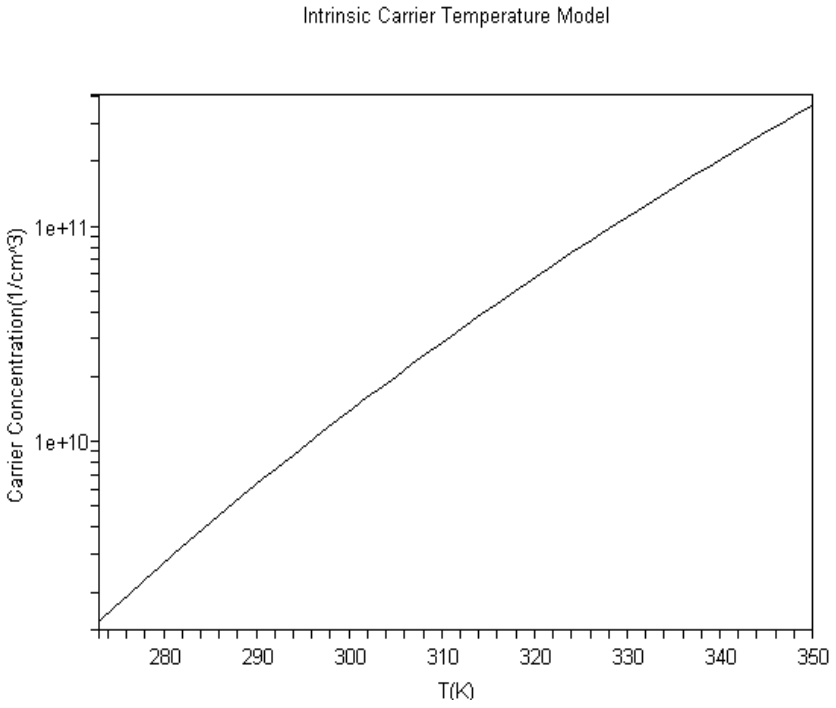

Figure 21: The intrinsic carrier concentration temperature dependence

5.1.2 Diffusion Coefficient for Electrons

From the Einstein relationship,

$$D_n = \frac{\mu kT}{q}, \tag{5.8}$$

therefore, the diffusion coefficient's dependence on temperature is captured not only by T in Equation (5.8) but also the electron mobility, μ, which is a monotonically decreasing function of temperature. Using an empirical relationship [25] for the mobility

$$\mu(T) = \left(\frac{2272.175}{T^{0.57}} + \frac{7.4 \cdot 10^{8}}{T^{2.33}\left(1 + 1.4153 \cdot 10^{-11} \frac{N_B}{T^{2.546}}\right)} \right), \tag{5.9}$$

where the doping concentration, N_B, is set to 10^{15} cm^{-2}, the reductions of mobility with temperature can be plotted (Figure 22).

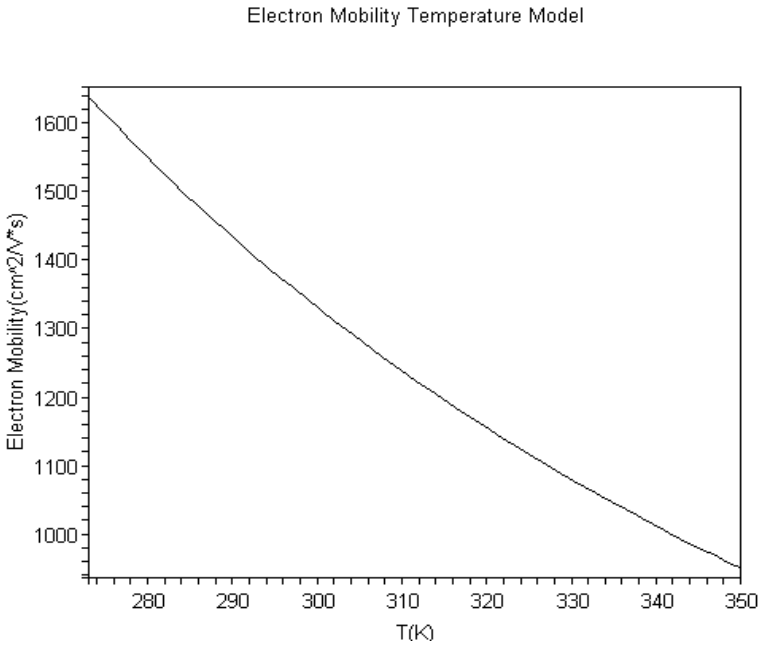

Figure 22: The electron mobility with empirical temperature dependence

The diffusion coefficient has a similar monotonic reduction with temperature, and is noted finally as

$$D_n(T) = \frac{\mu(T)kT}{q} \tag{5.10}$$

shown below.

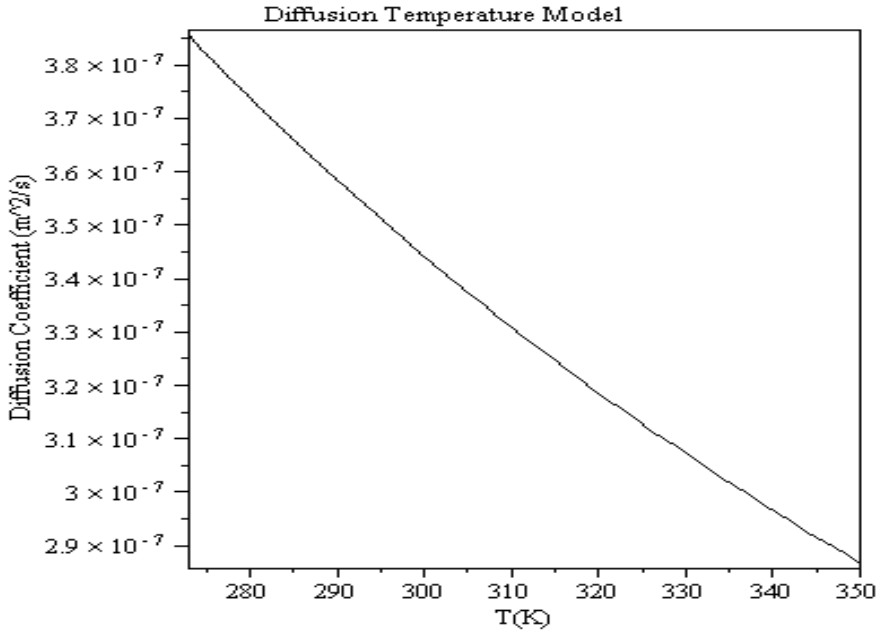

Figure 23: The diffusion coefficient plotted over temperature.

The functions expressed in Equations (5.7), (5.9), and (5.10) are used subsequently to model the dependence of base current on temperature. However, a more precise model for base current must be used to capture temperature effects on the low-injection base current as well.

5.1.3 Depletion region recombination current

In ideal forward bias operation, both the collector current and base current increase as a function of what Sah called Boltzmann's factor (qV_{be}/kT) [42],

$$I_c, I_{b,ideal} \propto \exp\left(\frac{qV_{be}}{kT}\right). \tag{5.11}$$

As described previously, in the traditional Gummel-Poon (GP) compact model for BJTs, the total base current under forward active bias (discussed in Section 3.1.3) is approximately

$$I_b \approx I_{b,ideal} + I_{SE} \exp\left(\frac{qV_{be}}{n_e kT}\right) \tag{5.12}$$

where the second term in the sum is I_{reb} [40]. As discussed in Chapter 3, emitter-base recombination current I_{reb}, is determined by two parameters: the base-emitter leakage emission coefficient (n_e), also known as the non-ideality factor, and the base-emitter leakage saturation current (I_{SE}). In most circuit simulator packages that use the GP model, I_{SE} and n_e, are constants, thereby making the natural log of I_{reb} expressible as a linear function of V_{be}, i.e.,

$$\ln\left(I_{reb}\right) \equiv \ln\left(I_{SE}\right) + \left(q/n_e kT\right)V_{be} \tag{5.13}$$

where the y-intercept is $\ln(I_{SE})$ and the slope, $S = d[\ln(I_{reb})]/dV_{be}$, is constant and equal to $q/n_e kT$ on a logarithmic graph. The experimental data and analysis presented here will demonstrate that forcing I_{SE} and n_e to be constants leads to an unphysical and inaccurate model of I_{reb}. Precise modeling of I_{reb} is critical to characterizing the impact of both radiation and temperature on BJTs.

When considering the change in base current over total dose it is beneficial to look at what is referred to as the excess base current, which is expressed as

$$\Delta I_B = I_B - I_{B_{prerad}} . \tag{5.14}$$

For TID, the excess base current is due to an increase in the surface recombination within the device, and can be approximated as

$$\Delta I_B \approx \Delta I_{reb} = I_{reb} - I_{reb,prerad} . \tag{5.15}$$

The magnitude of excess base current is determined by the combined effects of radiation-induced Si/SiO_2 interface traps (N_{it}), and of net positive oxide-trapped charge (N_{ot}) [43, 44]. Plots for experimentally obtained excess base current vs. V_{be} are shown in Figure 24 at various levels of total dose shown at room temperature.

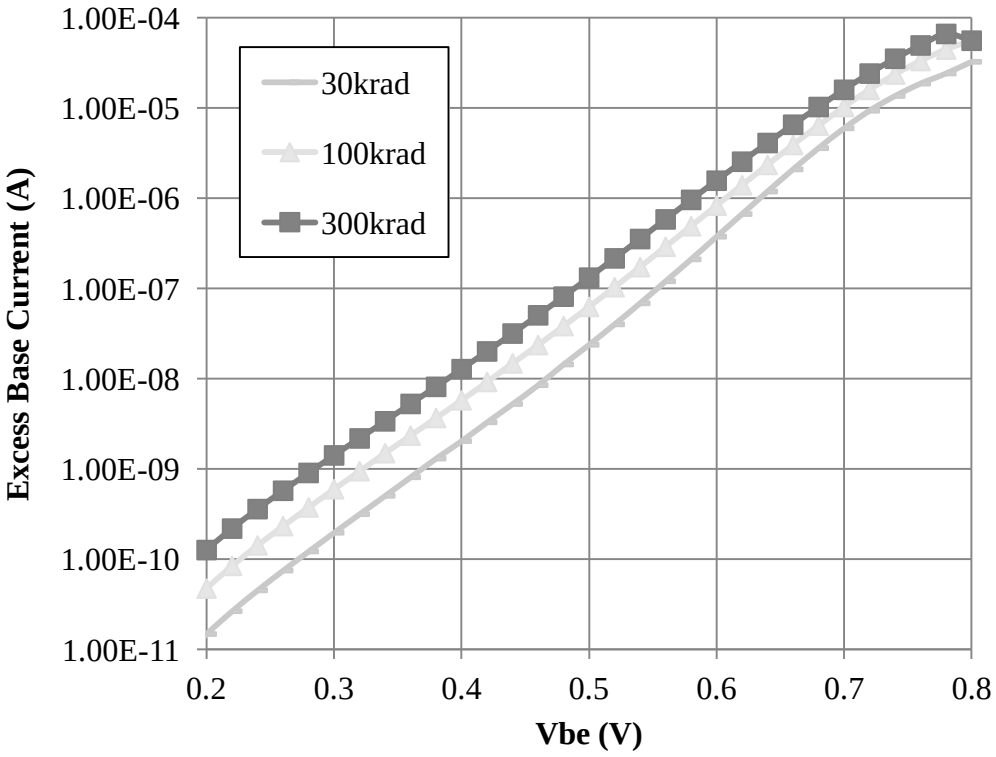

Figure 24: Excess Base Current

At low voltages (<0.5V), the slope is associated with an ideality factor greater than one, and it can be assumed that the entire radiation-induced excess base current is caused by increased emitter-base recombination. If TID damage can be assumed to be an increase due to increase surface recombination with the emitter-base depletion region, further simplifications can be made using an analytical model for recombination rate [35], or

$$\Delta I_{reb} = \Delta I_{reb,surface} + \Delta I_{reb,bulk} \approx \Delta I_{reb,surface} \tag{5.16}$$

A model for this is arrived at by deriving precise analytical equations for space-charge recombination current in p-n junctions, and finding the dependence

of recombination current on temperature and other device parameters [45, 46]. Ultimately this derivation is applied at the surface of the device, where *s* is the radiation dependent parameter.

The bias across the junction can be expressed as

$$qV_{be} = E_{Fn} - E_{Fp}, \tag{5.17}$$

where E_{Fn} and E_{Fp} are the quasi Fermi levels for electrons and holes respectively.

Quasi Fermi level connotations enable non-equilibrium expressions for electron and hole concentrations for devices, i.e.,

$$n(x) = n_i \exp\left(\frac{E_{Fn} - E_i(x)}{kT}\right), \tag{5.18}$$

and

$$p(x) = n_i \exp\left(\frac{E_i(x) - E_{Fp}}{kT}\right), \tag{5.19}$$

where $E_i(x)$ is the intrinsic Fermi level. Note that it is a fundamental property of p-n junctions that

$$n(x)\,p(x) = n_i^2 \exp\left(\frac{qV_{be}}{kT}\right) \quad \forall x. \tag{5.20}$$

By introducing a new energy variable, $q\phi(x) = E_{Fn} - E_i(x)$, then,

$$n(x) = n_i \exp\left(\frac{q\phi(x)}{kT}\right), \tag{5.21}$$

and using Equations (5.17) and (5.19) where $\phi(x)$ is the potential,

$$p(x) = n_i \exp\left(\frac{qV_{be}}{kT} - \frac{q\phi(x)}{kT}\right). \tag{5.22}$$

Using Equations (5.20), (5.21), (5.22), and performing some simplification, the SRH surface recombination rate [36] can be formulated as:

$$U(x) = \frac{n(x)\,p(x) - n_i^{\,2}}{\left(n(x) + p(x) + 2n_i\right)} \cdot s \,. \tag{5.23}$$

Since, in forward bias, the minority carrier concentrations are greater than n_i, we can re-write $U(x)$ as,

$$\begin{aligned} U(x) &= \frac{n_i \exp\left(\frac{qV_{be}}{2kT}\right)}{\exp\left(\frac{-qV_{be}}{2kT}\right)\left(\exp\left(\frac{q\phi(x)}{kT}\right) + \exp\left(\frac{qV_{be}}{2kT} - \frac{q\phi(x)}{kT}\right)\right)} \cdot s \\ &= \frac{1}{2}\frac{n_i \exp\left(\frac{qV_{be}}{2kT}\right)}{\cosh\left(\frac{q\phi(x)}{kT} - \frac{qV_{be}}{2kT}\right)} \cdot s \end{aligned} \,. \tag{5.24}$$

In order to calculate ΔI_b, $U(x)$ must be integrated from $x = 0$ to $x = x_d(V_{be})$. The main problem here is that $\phi(x)$ in the space-charge region is a non-linear function, which makes $\int U dx$ very difficult to evaluate in closed form. However, because of the sharply peaked structure of U (Figure 25), all that is required is a second function $U_1(x)$ defined such that

$$U_1(x) = U(x) \quad for\ x_m - \Delta x \le x \le x_m + \Delta x \tag{5.25}$$

for some small distance dx and such that

$$\int_{-\infty}^{\infty} U_1(x)dx \approx \int_{0}^{x_d(V_{be})} U(x)dx \,. \tag{5.26}$$

The change of limits in the integral assumes that the recombination that occurs outside of depletion region would be negligible and the limit of the function on both ends tends to zero. Furthermore, $\int U_1 dx$ must be able to be evaluated in a reasonable closed form. By defining U_1 as

$$U_1(x) \equiv \frac{1}{2} \frac{n_i \exp\left(\frac{qV_{be}}{2kT}\right)}{\cosh\left(\frac{q\phi_1(x)}{kT} - \frac{qV_{be}}{2kT}\right)} \cdot s \quad . \tag{5.27}$$

This expression is almost the same as $U(x)$ in Equation (5.24) except that the non-linear function $\phi(x)$ is replaced by a function $\phi_1(x)$ that satisfies the following three conditions:

1. $\phi_1(x)$ is linear
2. $\phi_1(x_m) = \phi(x_m) = V_{be}/2$
3. $d\phi_1(x)/dx\,|_{x = xm} = -\varepsilon(x_m)$

   (for a PNP device, the electric field at $x = x_m$)

With these conditions,

$$\phi_1(x) = \varepsilon(x_m)(x_m - x) + V_{be}/2 \quad , \tag{5.28}$$

Equation (5.27), for U_1, can now be reduced to

$$U_1(x) = \frac{1}{2} \frac{n_i \exp\left(\frac{qV_{be}}{2kT}\right)}{\cosh\left(\frac{q\varepsilon(x_m)(x_m - x)}{kT}\right)} \cdot s \quad . \qquad (5.29)$$

In order to provide a justification for the assumed equivalence in Equation (5.26), examine the plot, in Figure 25, of *U(x)* and $U_1(x)$ across the space-charge region of the p-n junction. As the figure indicates, $U_1(x)$ accurately reproduces *U(x)* near the peak, with an exact fit at x_m. Since the recombination drops quickly away from the peak, the integrals of *U* and U_1 are dominated by the recombination near the peak, and thus, are approximately equivalent.

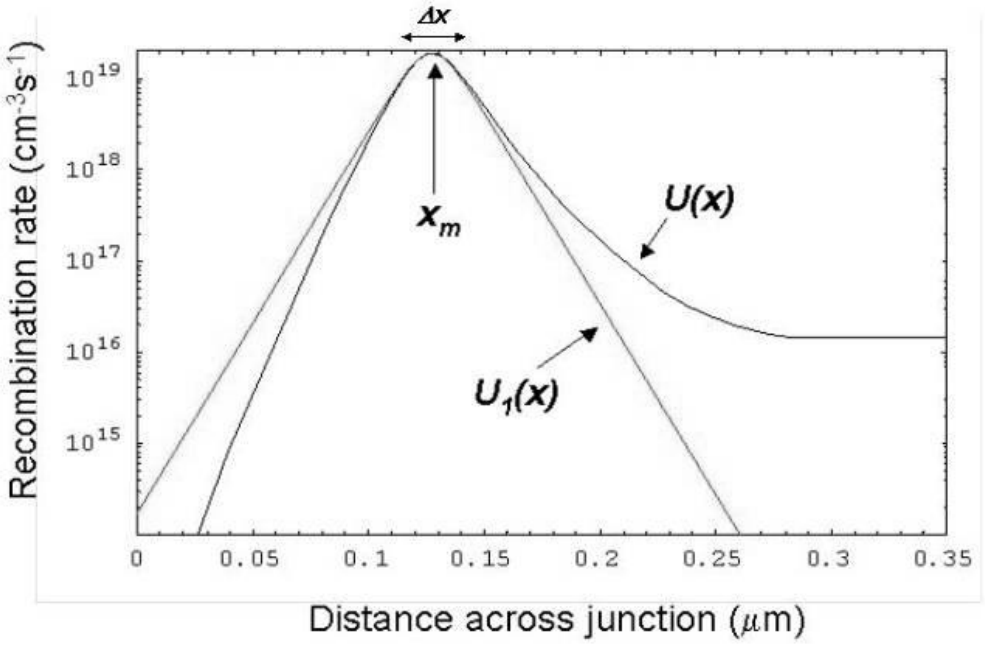

Figure 25: Plots of *U(x)* and $U_1(x)$ as a function of distance across the space-charge region of the p-n junction [38]

Unlike *U*, U_1 can be integrated analytically and thus a closed form

expression for surface recombination current can be derived as follows. Given Equations (5.23) and (5.26),

$$\Delta I_{reb,surface} \approx qP_E \int_{-\infty}^{\infty} U_1(x)\,dx$$
$$= \frac{qn_i P_E \Delta s}{2} \exp\left(\frac{qV_{be}}{2kT}\right) \int_{-\infty}^{\infty} \frac{dx}{\cosh\left(\frac{q\varepsilon(x_m)(x_m - x)}{kT}\right)}. \quad (5.30)$$

With some simple change of variables, specifically $y = -q\varepsilon(x_m)(x_m-x)/(kT)$ and $dx = kT/(q\varepsilon(x_m))dy$, and the identity

$$\int_{-\infty}^{\infty} \frac{dy}{\cosh(y)} = \pi, \quad (5.31)$$

$I_{reb,surface}$ can be written in a closed form:

$$\Delta I_{reb,surface} = \frac{n_i \pi kTP_E \Delta s}{2\varepsilon(x_m)} \exp\left(\frac{qV_{be}}{2kT}\right). \quad (5.32)$$

This equation specifically identifies the location of the electric field which will generate the precise answer, i.e., $\varepsilon = \varepsilon(x_m)$. All that remains is to derive an expression for $\varepsilon(x_m)$ that is a function of material parameters, processing variables, temperature, and bias conditions.

Evaluating Poisson's equation in one-dimension across a p-type emitter and n-type base and using appropriate boundary conditions gives

$$\frac{1}{q}\left(E_i(x) - E_i(x_m)\right) = \frac{qN_D}{2 \in_{Si}} (x - x_m)^2. \quad (5.33)$$

Furthermore, this can be expressed as,

$$\frac{1}{q}\left(E_i(x)-E_i(x_m)\right)=\phi(x)-\frac{V_{be}}{2}. \tag{5.34}$$

By combining Equations (5.33) and (5.34) while performing some rearrangements, a closed form expression for x_m can derived as

$$x_m = x-\sqrt{\frac{2\in_{Si}}{qN_D}\left(\phi(x)-\frac{V_{be}}{2}\right)}. \tag{5.35}$$

Then, given the basic assumptions regarding the p-n junction, i.e., the depletion approximation on a uniform, asymmetric step junction, we know

$$\phi(x)=\frac{kT}{q}\ln\left(\frac{N_D}{n_i}\right), \tag{5.36}$$

and from Poisson's,

$$\phi(x)=\frac{qN_D}{2\in_{Si}}\left(x-x_m\right)^2+V_{be}/2 \tag{5.37}$$

.

Therefore,

$$-\varepsilon(x=0)=\frac{\partial\phi(x=0)}{\partial x}=\frac{qN_D}{\in_{Si}}x_m. \tag{5.38}$$

By combining Eq. (5.35) and (5.36), the closed form expression for $\varepsilon(x_m)$ is expressed as

$$\varepsilon(x_m)=\sqrt{\frac{2qN_D}{\in_{Si}}\left(\frac{kT}{q}\ln\left(\frac{N_D}{n_i}\right)-\frac{V_{be}}{2}\right)} \tag{5.39}$$

Finally, by combining Equations (5.32) and (5.39), under the assumptions made in this thesis, the non-ideal base current component caused by recombination in the base-emitter space-charge region can be expressed as,

$$\Delta I_{reb,surface} = \frac{P_E kTn_i \pi \Delta s}{2} \frac{1}{\sqrt{\frac{2qN_D}{\in_{Si}}\left(\frac{kT}{q}\ln\left(\frac{N_D}{n_i}\right)-\frac{V_{be}}{2}\right)}} \exp\left(\frac{qV_{be}}{2kT}\right), \quad (5.40)$$

where the scale factor P_E that is the perimeter of the base-emitter junctions surface. Equation (5.12) reveals ΔI_{SE} to be a function of V_{be}, i.e.,

$$\Delta I_{SE} = \frac{P_E kTn_i \pi \Delta s}{2} \frac{1}{\sqrt{\frac{2qN_D}{\in_{Si}}\left(\frac{kT}{q}\ln\left(\frac{N_D}{n_i}\right)-\frac{V_{be}}{2}\right)}}, \quad (5.41)$$

The slope of the recombination current in the base-emitter space-charge region is

$$S = \frac{\partial\left(ln\left(\Delta I_{reb,surface}\right)\right)}{\partial V_{be}} = \frac{dln\left(\Delta I_{SE}\right)}{\partial V_{be}} + \frac{q}{n_e kT} \quad (5.42)$$

To simplify, define a function γ that is dependent on V_{be} in the following relation:

$$\gamma\left(V_{be}\right) = \frac{2qN_D}{\in_{Si}}\left(\frac{kT}{q}\ln\left(\frac{N_D}{n_i}\right)-\frac{V_{be}}{2}\right). \quad (5.43)$$

Then,

$$\ln\left(\Delta I_B\right) \approx \ln\left(\Delta I_{reb,surface}\right) = \ln\left(\frac{P_E kTn_i \pi \Delta s}{2}\right) + \frac{qV_{be}}{2kT} - \frac{1}{2}\ln\left(\gamma\right) \quad (5.44)$$

and the slope can be represented as

$$S = \frac{\partial \ln\left(\Delta I_B\right)}{\partial V_{be}} = \frac{q}{2kT} - \frac{1}{2\gamma}\frac{\partial \gamma}{\partial V_{be}}. \quad (5.45)$$

Moreover,

$$\frac{\partial \gamma}{\partial V_{be}} = -\frac{qN_D}{\in_{Si}}. \quad (5.46)$$

So the model for the slope reduces to:

$$S = \frac{q}{2kT} + \frac{1}{4\left(kT/q \cdot \ln\left(N_D/n_i\right) - V_{be}/2\right)}. \qquad (5.47)$$

Then the more precise ideality factor is related to this slope as:

$$n_e = \frac{q}{SkT}. \qquad (5.48)$$

This analytical expression is a much more accurate approximation of the log-linear slope of ΔI_B, if the excess base current is solely caused by increase recombination with interface traps in the emitter-base space charge region (which is a very reasonable assumption for BJTs degraded by ionizing radiation exposure. Shown in Figure 26 is the predicted slope of ΔI_B as a function of base-emitter voltage. Using this model it can be seen that the slope is dependent on bias and this slope is always higher [36] than the constant 19.3 V^{-1} (non-ideality factor of 2) used as the room temperature default in most circuits simulators.

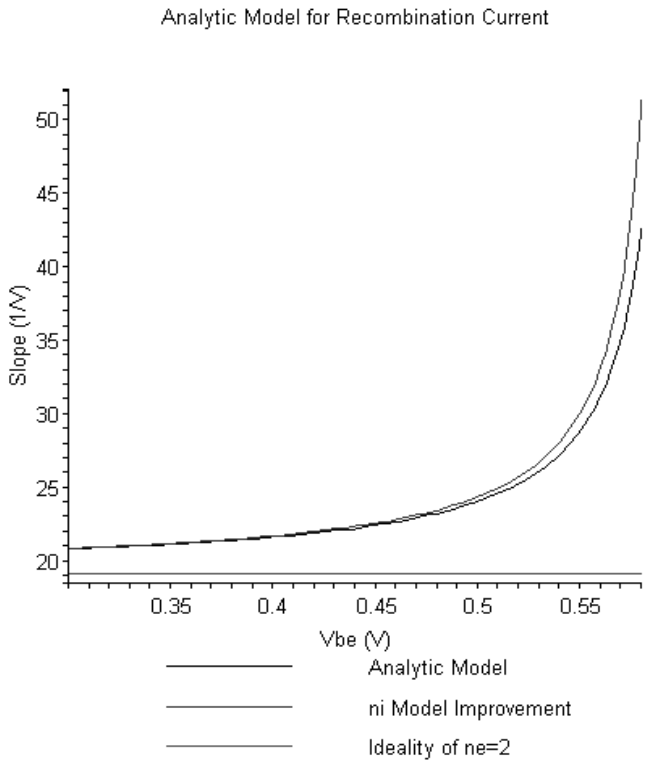

Figure 26: Model of recombination current slope

This model can be further improved for temperature variation using the $n_i(T)$ representation from Equation (5.7). The result, shown in Figure 26, shows that having n_i as a function of temperature predicts an inflection of the base current at a lower V_{be}, and is also slightly higher for all V_{be}.

The impact of base resistance must also be included in the model due to the low doping of the device material tested (~10^{15} cm^{-2}). This low doping profile results in an internal base resistance, r_b, which alters the junction bias from base to emitter. When r_b is included, the internal junction bias becomes

$$v_{be} = V_{be} - I_b r_b . \tag{5.49}$$

For the model of ideality factor in this these devices a base resistance was assumed to be on the order of 30 kohms due to the known values of doping and base depth.

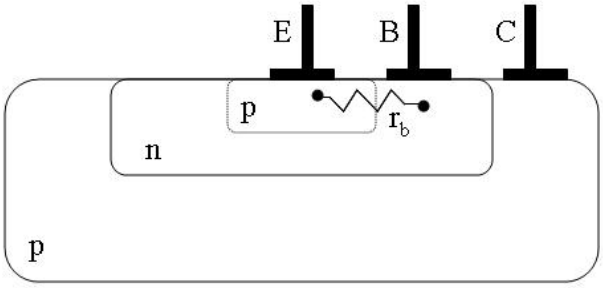

Figure 27: Base resistance shown

To model the internal base resistance's effect, the reading of base current for a particular bias is multiplied by this temperature dependant value of resistance, and subtracted from the value of V_{be}.

Figure 28 plots the ideality factor as a function of V_{be} over four temperatures. The reductions of the ideality factor for low V_{be} is determined by Equation (5.47). The increase in the response at the higher V_{be} levels is a signature of the base resistance effect. Also, included on the figure are experimental results from two chips measured at the four temperatures. As the plots indicate, the model fits well to the experimental data, as it is inversely proportional to the derivative of the base current.

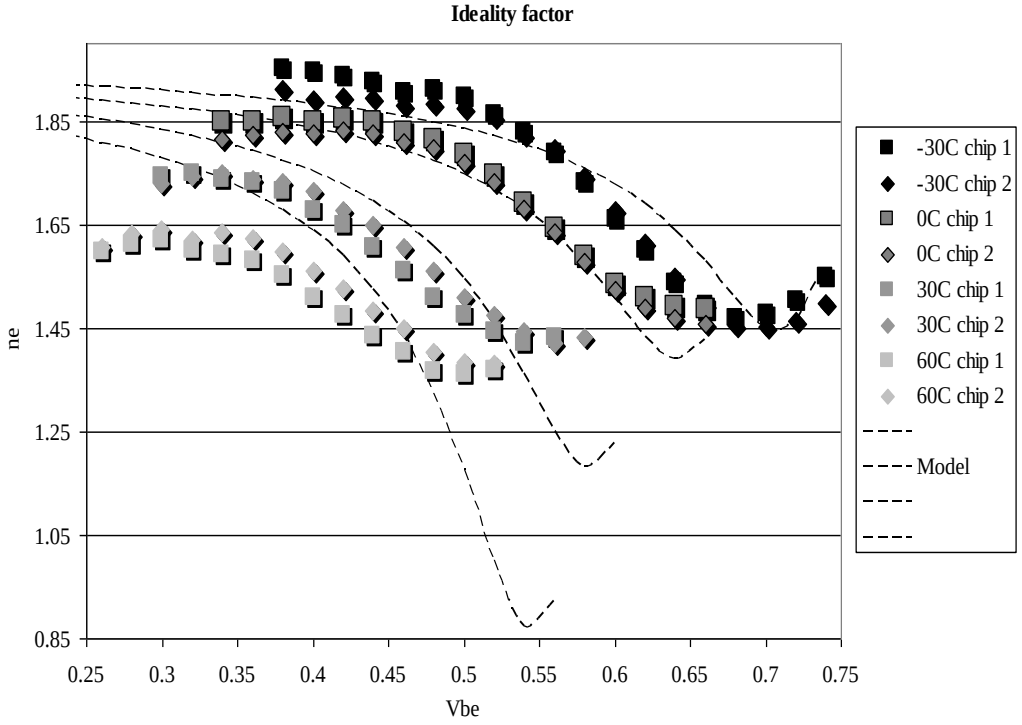

Figure 28: Ideality factor model for temperatures, shown with post-rad data

It is then the intention to use these temperature models that fit experimental ideality factors fairly well to justify the extraction of the surface recombination velocity which is dependent on the radiation degradation that the device accrues. In doing so, the actual degradation regardless of what temperature the device readings are taken at is known. The effects of radiation can then be isolated by knowing only the temperature and the slope of the base current of the devices in question.

5.2 Isolation of effects

The following section describes one method for isolating effects of temperature and radiation damage on BJTs. Extracting the surface recombination

velocity within the device is the goal, while accounting for any temperature dependence of parameters such that the change in surface velocity is not exaggerated or diminished by temperature effects. While the ideality factor is able to be matched for low and elevated temperatures, it is elevated temperature that clouds the effect of base current increase due to TID. For that instance the SRV must be extracted.

Extraction of Surface Recombination Velocity Over Temperature

The process of extracting the surface recombination velocity begins with analyzing the Gummel curves of the device and utilizing the previous temperature models. Surface recombination velocity shifts due to the introduction of interface traps along the base surface of the lateral device [36]. The relation of the two is defined as

$$s = \sigma_s v_{th} N_{it} \tag{5.50}$$

Where σ_s is the carrier capture cross section at the surface, v_{th} is the thermal velocity and N_{it} is the interface trap density.

Assuming the emitter-base recombination is responsible for increased base current due to TID one can state

$$\Delta I_B = \Delta I_{SE} \cdot \exp\left(\frac{qV_{be}}{2kT}\right). \tag{5.51}$$

Using the derived analytic model of recombination rate [38] where,

$$\gamma\left(V_{be}\right) = \frac{2qN_D}{\in_{Si}}\left(\frac{kT}{q}\ln\left(\frac{N_D}{n_i}\right) - \frac{V_{be}}{2}\right). \tag{5.52}$$

The change in current is then dependent on emitter-base bias unlike the Gummel-Poon model:

$$\Delta I_{SE} = \Delta I_{SE_0} \cdot \left(\gamma(V_{be})\right)^{-1/2} \quad . \tag{5.53}$$

The excess base current can be found at a given bias from the experimental data in Equation (5.14) and related to the bias dependent model, i.e.,

$$\Delta I_B = \Delta I_{SE_0} \cdot \exp\left(\frac{qV_{be}}{2kT} - \frac{1}{2}\ln(\gamma)\right). \tag{5.54}$$

The parameter change of interest for ionizing radiation dose analysis is the surface recombination velocity, Δs:

$$\Delta I_{SE_0} = \frac{P_E kTn_i \pi}{2} \Delta s \quad , \tag{5.55}$$

where P_E is the perimeter of the emitter. The change in surface recombination velocity can then be backed out of the base current data, and proportionally the interface traps. The final representation of the surface recombination velocity as a function of excess base current, temperature, and base-emitter bias is shown in Equation(5.56):

$$\Delta s = \frac{2\Delta I_B}{kTn_i(T)\pi P_E \sqrt{\frac{2qN_D}{\in_{Si}}\left(\frac{kT}{q}\ln\left(\frac{N_D}{n_i(T)}\right) - \frac{V_{be}}{2}\right)} \cdot \exp\left(\frac{-qV_{be}}{2kT}\right)}. \tag{5.56}$$

Plotting this extraction (Figure 29) shows that as expected more damage or trapped charge is present for increasing dose. It can also be seen that the SRV extraction changes over V_{be}, having a peak between 0.6V and 0.8V. This peak is assumed to correlate with internal base resistance and the drift component of

current overtaking that of recombination, thus higher voltages are assumed to not be associated with the current changes due to radiation induced degradation.

Typically the SRV is extracted where the excess base current changes slope, as done in previous work [44], where recombination current is at a maximum, or at a V_{be} determined to be the transition voltage. However, using the method described in this thesis, SRV is extracted for all V_{be} below this point, noting that the radiation induced change in base current would dominate at these voltage levels. The plots used for this analysis show agreement of SRV for V_{be} up to the turning point of excess base current that would be chosen (between 0.45 and 0.65V, see Figure 24), however this step is left out to support the validity of the models used, not to show dependence of SRV on V_{be}.

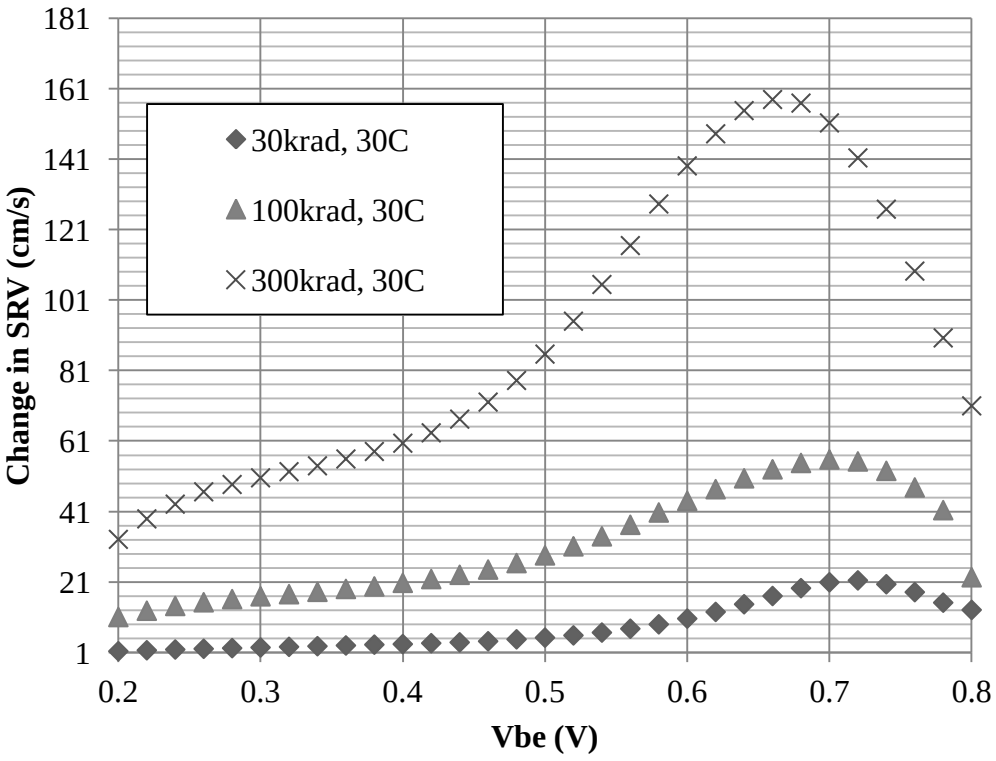

Figure 29: Surface recombination velocity changes over TID

The next objective is to characterize these surface recombination velocity changes over temperature. First, verification of the models comes when plotting the change in surface recombination velocity for various temperatures pre-rad, shown in Figure 30. When pre-rad part readings are compared to that of an irradiated, we see that the variation of temperature is accounted for, and properly removed, i.e. no dose, no change in SRV and therefore no additional interface traps. The small variations of SRV for the 0krad at higher V_{be} may come from errors in the measurement or changes in current not due to recombination. Their order of magnitude differences from the dosed parts hold that this method can be accurately used.

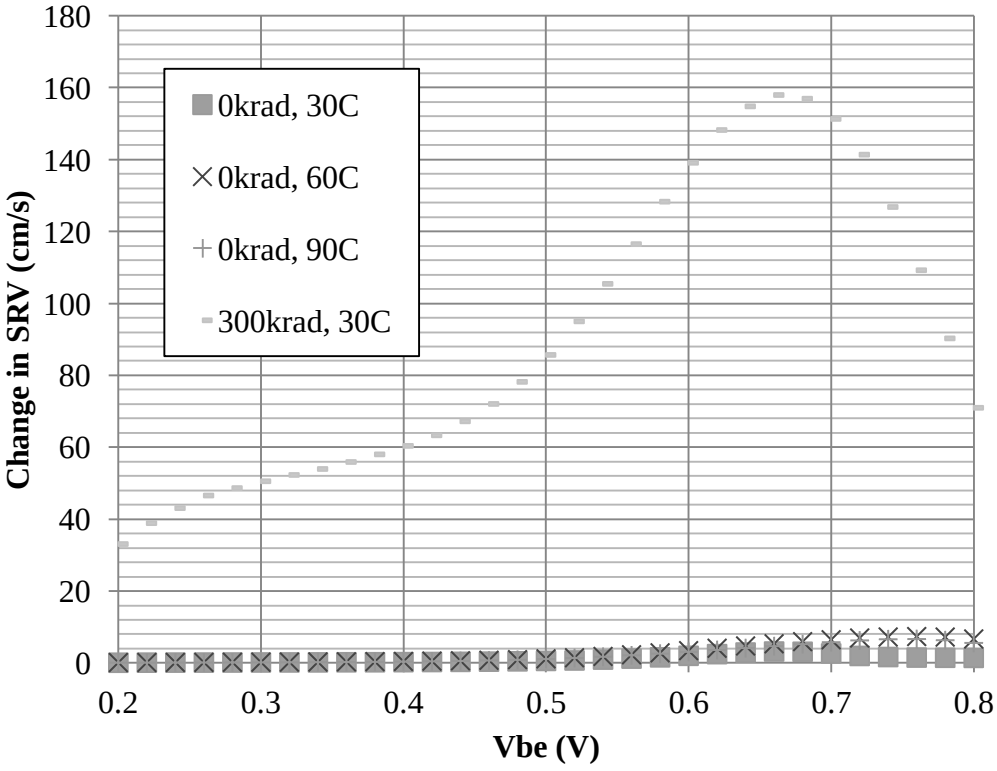

Figure 30: Surface recombination velocity changes over temperature, pre-rad

Next, the readings post-rad at temperature are taken into account, noting that any change in SRV is solely from radiation degradation. It would be expected that SRV extraction would be constant for any temperature; however, this would not agree with the physical phenomena of annealing [14]. In accordance, the data show much lower changes in SRV at elevated temperatures, which agrees with our understanding of ionization effects and interface traps annealing. This was confirmed with another room temperature measurement taken after the part was heated for readings, shown in Figure 31. This output data agrees with the 90 degree result.

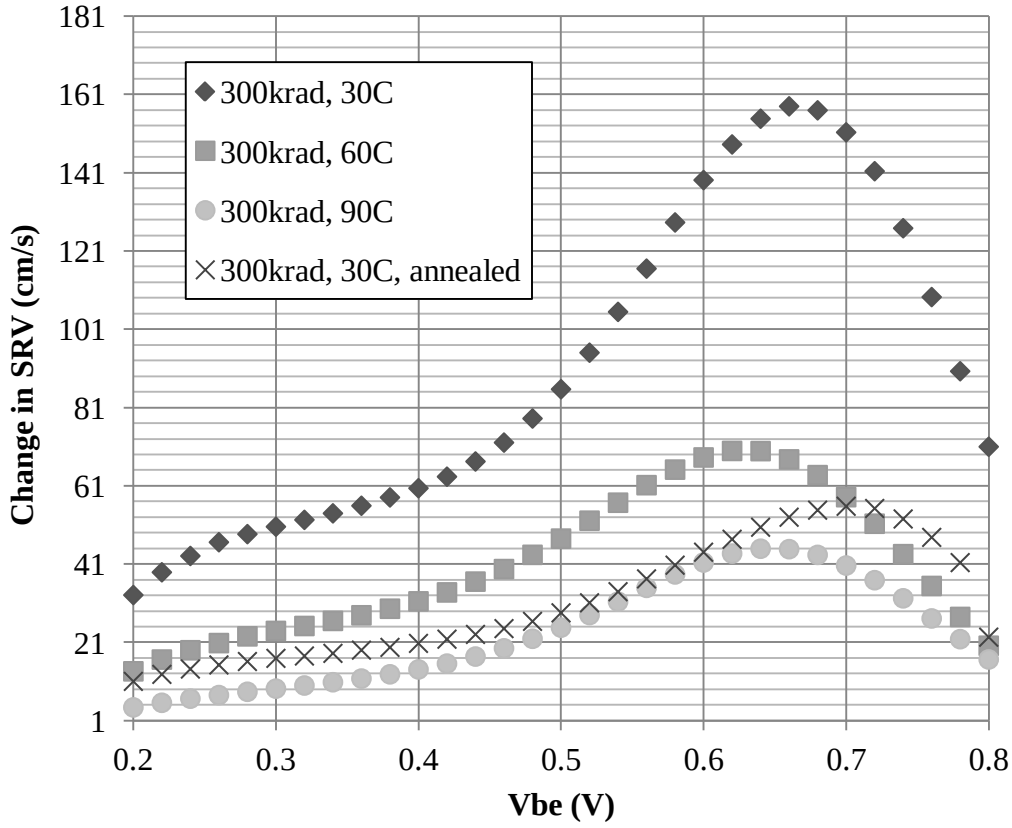

Figure 31: Surface recombination velocity changes over temperature, post-rad with annealing

Once plotted, the effect on the SRV below ~0.5V can be seen only as dependence on the number of interface traps or degradation due to ionization. With the proper temperature models, SRV extraction can be used to single out the radiation response independent of temperature so long as the temperature at which the readings were taken is known.

6 CONCLUSION

The use of semiconductor devices in hostile environments demands more understanding of these devices and how they react to the many variables they encounter, particularly on spaceflight applications. Without this understanding, the degradation of the part itself cannot be predicted accurately nor anticipated.

The specific study of base current shifts in bipolar junction transistors is not applicable to most commercial applications. However, when dealing with BJTs that operate in space radiation environments, increases in base current caused by ionizing total dose exposure can become a tremendous problem. Inevitably, this leads to failure in mission systems that use these devices. That said, the temperature effects on the device can amplify the radiation response and lead to premature failures or unexpected readings from devices used for instrumentation. The key is to know the environment, and expect its variation.

This thesis presents not only an understanding of the environmental hazards, but the specific device operation under normal circumstances. This was done in an effort to later characterize the device response to radiation and temperature separately during ground based experiments.

Modeling the recombination current in a p-n junction gives a valid explanation of why the base current slope is always greater than the ideal from the GP model. Measurements taken from a BJT support this and show the slope to be higher and dependant on V_{be}. BJT base current readings from varying temperature conditions can be compared more accurately with an understanding of the change in base current due only to temperature. The normalization of this effect is done

so through empirical studies of device parameters and base current slope. By first mapping the base current with an appropriate model of ideality factor, extracting the change in surface recombination velocity for datasets can be compared if adequate temperature readings are taken.

The mathematical models in this thesis can be used to better understand radiation and temperature effects on the base current in BJTs. The extraction of information from these devices can be used as a reference for devices remotely sensing their temperature, to have a better understanding of the dose the part has accrued regardless of that temperature. This separation of variables allows for better approximation of part function and understanding of abrupt changes in environment while in-situ.

The work done in this thesis can be furthered and applied in many ways. Some benefit and accuracy can be added by utilizing numeric solutions to the surface recombination rate instead of the analytic representation that was derived. In doing so, more confidence in the extraction would allow application to more complex devices as well as the basic device parameters are known. Another step in the forward direction would be to take multiple readings abruptly at elevated temperature such that annealing effects can be better recorded.

Separating these effects is essential in real world application and can determine the life of a system intended for space operation. Until we understand how temperature and radiation individually affect the device performance we cannot say whether the compound effect will be catastrophic.

REFERENCES

1] D.M. Sawyer and J.I. Vette, AP-8 Trapped Proton Environment for Solar Maximum and Solar Minimum, NSSDC/WDC-A-R&S, 76-06, NASA Goddard Space Flight Center, Greenbelt, MD, Dec. 1976.

2] J.I. Vette, The AE-8 Trapped Electron Environment, NSSDC/WDC-A-R&S 91-24, NASA Goddard Space Flight Center, Greenbelt, MD, Nov. 1991.

3] W. Baumjohann and R. A. Treumann, Basic Space Plasma Physics, Covent Garden, London, Imperial College Press, 1997, pp 5-46.

4] http://www.spenvis.oma.be/

5] R.C. Reedy, "Radiation Threats from Huge Solar Particle Events", in Proc. Conf. High Energy Radiation. Background in Space, edited by P.H. Solomon, NASA Conference Publication 3353, pp.77-79, 1997.

6] T. F. Tascione, Introduction to the Space Environment, Malabar, FL: Krieger Publishing Company, 1994.

7] C.E. McIlwain, "Coordinates for Mapping the Distribution of Magnetically Trapped Particles", J. Geophys. Res., Vol. 66, 3681-3691, 1961.

8] Living with a Star Space experiment testbed Experiment Accommodations & Requirements Specification (SEARS), LWSSET-SPEC-0001, Goddard Space Flight Center, Greenbelt, MD, 2004, unpublished.

9] Paul E. Dodd, "Basic Mechanisms for Single-Event Effects," Notes from IEEE Nuclear and Space Radiation Effects Conference Short Course, Norfolk, VA, 1999.

10] Edward L. Petersen, "Single Event Analysis and Prediction," Notes from IEEE Nuclear and Space Radiation Effects Conference Short Course, Snowmass, CO, 1997.

11] F.B. McLean, H.E. Boesch and T.R. Oldham, "Electron-Hole Generation, Transport, and Trapping," in Ionizing Radiation Effects in MOS Devices & Circuits," Ed. By T.P. Ma and P.V. Dressendorfer, John Wiley and Sons, 1989.

12] D. R. Ball, R. D. Schrimpf, H. J. Barnaby, "Separation of Ionization and Displacement Damage Using Gate-Controlled Lateral PNP Bipolar Transistors", IEEE Trans. Nucl. Sci., Vol. 49, No. 6, pp. 3185-3190, 2002.

13] R. L. Pease, “Total Ionizing Dose Effects in Bipolar Devices and Circuits,” IEEE Trans. Nucl. Sci., vol. 50, pp. 539-551, 2003.

14] T. Oldham, “Ionizing Radiation Effects in MOS Oxides,” World Scientific, Singapore, 1999.

15] X. J. Chen, H. J. Barnaby, R. D. Shrimpf, D. M. Fleetwood, R. L. Pease, D. G. Platteter, and G. W. Dunham, “Nature of Interface Defect Buildup in Gated Bipolar Devices Under Low Dose Rate Irradiation,” IEEE Trans. Nucl. Sci., Vol. 53, pp. 3649-3654, Dec 2006

16] Pease, R.L.; Platteter, D.G.; Dunham, G.W.; Seiler, J.E.; Barnaby, H.J.; Schrimpf, R.D.; Shaneyfelt, M.R.; Maher, M.C.; Nowlin, R.N., "Characterization of enhanced low dose rate sensitivity (ELDRS) effects using Gated Lateral PNP transistor structures," IEEE Trans. on Nucl. Sci., vol.51, no.6, pp. 3773- 3780, Dec. 2004

17] A. H. Johnston, B. G. Rax, and C. I. Lee, “Enhanced damage in linear bipolar integrated circuits at low dose rate,” IEEE Trans. Nucl. Sci., vol. 42, pp. 1650-1659, 1995.

18] T. L. Turflinger, A. B. Campbell, W. M. Schmeichel, R. J.Walters, J. F. Krieg, J. L. Titus, M. Reeves, P.W. Marshall, and R. L. Pease, “ELDRS in Space: An Updated and Expanded Analysis of the Bipolar ELDRS Experiment on MPTB,” IEEE Trans. Nucl. Sci., vol. 50, pp. 2328-2334, Dec 2003.

19] J. L. Titus, W. E. Combs, T. L. Turflinger, J. F. Krieg, H. J. Tausch, D. B. Brown, R. L. Pease, and A. B. Campbell, "First Observations of Enhanced Low Dose Rate Sensitivity (ELDRS) in Space: One Part of the MPTB Experiment," IEEE Trans. Nucl. Sci., NS-45, pp. 2673-2680, Dec 1998.

20] J. L. Titus, D. Emily, J. F. Krieg, T. Turflinger, R. L. Pease, and A. Campbell, “Enhanced low dose rate sensitivity (ELDRS) of linear circuits in a space environment,” IEEE Trans. Nucl. Sci., vol. 46, pp. 1608-1615, 1999.

21] http://www.srim.org

22] J.F. Ziegler, J.P Biersack, and U Littmark, “The Stopping and Range of Ions in Matter,” Pergamon Press, New York, 1996.

23] J. R. Srour, C. J. Marshall, and P. W. Marshall, “Review of Displacement Damage Effects in Silicon Devices,” IEEE Trans. Nucl. Sci., 50(3): pp. 653-670, June 2003.

24] Neudeck, Gerold W., The Bipolar Junction Transistor, Modular Series on Solid State Devices, Volume III, Reading, MA, Addison-Wesley, 1989.

25] M. Shur, Physics of Semiconductor Devices, Upper Saddle River, NJ: Prentice Hall, pp. 239-309, 1990.

26] H. J. Barnaby, *et al*., "Minimizing gain degradation in lateral PNP bipolar junction transistors using gate control," IEEE Trans. Nucl. Sci., 46(6): pp. 1652-1659, 1999.

27] A. H. Johnston, G. M. Swift, and B. G. Rax, "Total dose effects in conventional bipolar transistors and linear integrated circuits," IEEE Trans. Nucl. Sci., 41: pp. 2427-2436, 1994.

28] R. L. Schrimpf, "Recent Advances in Understanding Total-Dose Effects in Bipolar Transistors," 1996 IEEE Trans. Nucl. Sci., vol. 43, No. 3, pp. 787-796, 1996.

29] D. Schroder, "Lecture #15:Bipolar Junction Transistors - 1," class notes for EEE 532, Department of Electrical Engineering, Arizona State University, Fall 2004.

30] D. M. Schmidt, A. Wu, R. D. Schrimpf, D. M. Fleetwood, and R. L. Pease, "Modeling ionizing radiation induced gain degradation of the lateral PNP bipolar junction transistor," IEEE Trans. Nucl. Sci., vol. 43, pp. 3032-3039, 1996.

31] P. Cazenave, P. Fouillat, X. Montagner, H. Barnaby, R. D. Schrimpf, L. Bonora, J. P. David, M. C. Calvet, and P. Calvel, "Total Dose Effects on Gate Controlled Lateral PNP Bipolar Junction Transistors," IEEE Trans. Nucl. Sci., vol. 45, pp. 2577-2583, 1998.

32] M. R. Shaneyfelt, R. L. Pease, M. C. Maher, J. R. Schwank, S. Gupta, P. E. Dodd, and L. C. Riewe, "Passivation Layers for Reduced Total Dose Effects and ELDRS in Linear Bipolar Devices", IEEE Trans. Nucl. Sci. NS-50, No.6, 1784-1790, December 2003.

33] H. J. Barnaby, Arizona State University, Tempe, AZ, private communication, Fall 2006.

34] http://ecee.colorado.edu/~bart/book/book/chapter5/ch5_4.htm

35] H. J. Barnaby, et al., "Analytical Model for Proton Radiation Effects in Bipolar Devices," IEEE Trans. Nucl. Sci., 2002. 49(6): p. 2643-2649.

36] M. Y. Ghannam and R. P. Mertens, "Surface Recombination Current with a Nonideality Factor Greater than 2," IEEE Elec. Dev. Letters, vol. 10, pp. 242-244, June 1989.

37] D. A. Johns and K. Martin, Analog Integrated Circuit Design, New York, NY: Wiley, pp. 196-200, 1997.

38] H. J. Barnaby and B. Vermeire, "An analytical expression for recombination current in base-emitter space-charge region," Unpublished.

39] http://www.sbfisica.org.br/bjp/files/v40_120.pdf

40] G. Massobrio, and P. Antognetti, "Semiconductor device modeling with SPICE," second ed. 1993, New York: McGraw-Hill Inc.

41] http://www.ujp.bitp.kiev.ua/files/file/papers/51/6/510611p.pdf

42] R. F. Pierret, Advanced Semiconductor Fundamentals, Upper Saddle River, NJ: Prentice Hall, pp. 78-168, 2003.

43] S. L. Kosier, R. D. Schrimpf, A. Wei, M. DeLaus, D. M. Fleetwood, and W. E. Combs, "Effects of Oxide Charge and Surface Recombination Velocity on the Excess Base Current of BJTs," in Proc. IEEE Bipolar/BiCMOS Circuits and Technology Meeting, pp. 211-214, 1993.

44] S. L. Kosier, R. D. Schrimpf, D. M. Fleetwood, M. DeLaus, R. L. Pease, W. E. Combs, A. Wei, and F. Chai, "Charge separation for bipolar transistors," IEEE Trans. Nucl. Sci., vol. 40, pp. 1276-1285, 1993.

45] J. Boch, F. Saigné, R. D. Schrimpf, D. M. Fleetwood, R. Cizmarik, and D. Zander, "Elevated Temperature Irradiation at High Dose Rate of Commercial Linear Bipolar ICs," IEEE Trans. Nucl. Sci., vol. 51, pp. 2903-2907, Oct. 2004

46] J. C. S. Woo, J. D. Plummer, J. M. C. Stork "Non-Ideal Base Current in Bipolar Transistors at Low Temperatures," IEEE Elec. Dev. Letters, vol. 34, pp. 130-138, Jan. 1987.